Clays and Clay Minerals, Vol. 59, No. 1, 75–94, 2011.

MINERALOGICAL AND GEOCHEMICAL PROPERTIES OF THE Na- AND Ca-BENTONITES OF ORDU (NE TURKEY)

MUAZZEZ ÇELIK KARAKAYA*, NECATI KARAKAYA, AND ŞUAYIP KÜPELI

Selçuk Universitesi Muh.-Mim. Fakültesi Jeoloji Mühendisliği Bölümü, Konya, 42079, Turkey

Abstract—A number of different types of bentonite deposits formed by hydrothermal alteration and diagenetic processes are to be found in the Ordu area of the Eastern Black Sea region. The Ca- and Na-bentonite deposits are related to Upper Cretaceous tholeitic to calc-alkaline volcanites, predominantly dacite and andesite, and also include rhyodacite with lesser basalt and their pyroclastic equivalents. In the present study, dacite (PR1), perlite (PR2), moderately altered rocks (MPR), and Na- and Ca-bentonites were studied to describe and compare their mineralogical and geochemical properties and their conditions of formation by means of X-ray diffraction, optical microscopy, scanning electron microscopy, and chemical analytical techniques.

Ca-bentonites, except for smectite, contain opal-CT, feldspar, biotite, and rarely pyrite, while Na-bentonites contain smectite and less feldspar, opal-CT, kaolinite, and illite.

Progressive alteration of the PR2 caused depletion in K_2O and Na_2O and enrichment in MgO and CaO in all of the Ca-bentonite samples. Na_2O was depleted in all of the Na-bentonites and in most of the MPR. The medium and heavy rare earth elements (*MREE* and *HREE*) show mass gain or mass loss in the Na-bentonites. The *HREE* show nearly immobile behavior in the Ca-bentonites. The rare earth elements (*REE*) and transition elements (TRE) mostly gained mass in the Ca-bentonites in contrast to Na-bentonites. Large-ion lithophile elements (LILE) are strongly depleted in all of the bentonites. The *LREE*, *MREE*, and *HREE* were strongly depleted in most of the MPR samples. TiO_2, Lu, Tm, and Tb show immobile behavior in all samples.

PR1 exhibits a slightly positive Eu anomaly. Two MPR samples show slightly positive Eu anomalies (1.03, 1.13), and one Na-bentonite sample displays a slightly positive Eu anomaly (1.04). Most of the Na-bentonites have weakly negative Eu anomalies, whereas perlite and the Ca-bentonite have a strongly negative Eu anomaly. The PR1, PR2, MPR, and Na-bentonite present a positive Ce anomaly, and the Ca-bentonite shows a moderately negative Ce anomaly. The Ca-montmorillonites are mainly hydrothermal in origin and derived from alteration of volcanoclastic material *in situ* and/or in the subaerial environment. The Na-montmorillonites formed by alteration and diagenesis of volcanoclastic material in the sedimentary basin.

Key Words—Bentonite, Genesis, Geochemistry, Hydrothermal Alteration, Mass Balance, Ordu, Smectite, Trace Elements, Turkey.

INTRODUCTION

Bentonites form from volcanic glass and consist predominantly of clay minerals of the smectite group. Bentonite forms by one of the following three processes: (1) diagenetic alteration of volcanic glass; (2) hydrothermal alteration of volcanic glass; and (3) formation of smectite-rich sediments in salt lakes and sabkha environments, usually from dissolution of detrital smectites, which is often associated with sepiolite and/or palygorskite (Christidis and Warren, 2009). Smectite formation from volcanic materials mostly involves *in situ* hydrolysis of the materials in sea or brackish or fresh waters (Grim, 1968; Millot, 1970; Grim and Güven, 1978; Chamley, 1989; Velde, 1995). Regardless of the formation process, leaching of alkali elements and large $(Mg^{2+})/(H^+)$ ratios are required to form smectites rather than zeolites during the alteration of volcanic glass (Senkai *et al*., 1984; Christidis, 1998). Many bentonite deposits of hydrothermal origin are to be found in Algeria, Argentina, Australia, Greece, Italy, Japan, Hungary, Spain, and Turkey (Christidis *et al.*, 1995; Christidis, 1998; Terkado and Fujitani, 1998; Çelik *et al.*, 1999; Yalçın and Gümüşer, 2000; Lombardi *et al.*, 2003; Caballero *et al.*, 2005; Ddani *et al.*, 2005; Arslan and Abdioğlu, 2005; Yıldız and Dumlupınar, 2009). Some bentonites consist of pure montmorillonite. The composition of montmorillonite varies considerably in terms of the number of exchangeable cations in different bentonite deposits. Ca^{2+} is the dominant exchangeable cation in most montmorillonite samples. When Ca^{2+} is the dominant exchangeable cation, Mg^{2+} is frequently present as an exchangeable ion in relatively small amounts. Na^+ is the dominant ion in montmorillonite in only a small number of cases. Wyoming bentonite, the main example of a Na-bentonite (Grim, 1968), formed by alteration of volcanic ash reacted with seawater in pore fluids after burial (Hora, 1998).

* E-mail address of corresponding author:
mzzclk@hotmail.com
DOI: 10.1346/CCMN.2011.0590109

The investigation area in the west of the Eastern Pontides, NE Turkey (Figure 1), represents the eastern part of the metallogenic province of the Black Sea. The mineralization is related to intermediate volcanic rocks that are crosscut by acidic magmatic rocks associated with widespread hydrothermal alteration, clay mineralization, and deposition (Çağatay, 1993; Çelik *et al*., 1999). Clay occurrences, some of which are of economic interest, are located within the alteration haloes around the massive sulfide deposits in different parts of the province. Hydrothermal alteration processes are affected by different types of post-volcanic solutions, especially on the hanging walls and footwalls of the massive sulfide deposits (Grim and Güven, 1978; Çağatay, 1993; Çelik *et al.*, 1999; Karakaya *et al.*, 2001a, 2001b; Karakaya *et al.*, 2005). Alunite and kaolin deposits in the southeastern part of the study area resulted from intense hydrothermal alteration of the volcanic rocks (Karakaya and Karakaya, 2001a; Karakaya *et al.*, 2007). The properties and genesis of different clay deposits, including two types of Ca-bentonite, have been studied by several authors (*e.g.* Çelik *et al.*, 1999; Yalçın and Gümüşer, 2000; Arslan and Abdioğlu, 2005). Little information is available, however, about the mineralogical and geochemical characteristics and origins of the bentonite deposits, especially for the Na-bentonite in the Ordu area. The bentonitic clay deposits cover an area of ~150 km^2. The objectives of this research were: (1) to describe the properties of the bentonitic clay deposits in the Ordu area; (2) to study compositional variations in the bentonite; and (3) to explain the conditions of formation of the bentonite. Elemental behaviors during alteration are also reported.

GEOLOGIC SETTING

The northeastern part of Turkey, also known as the Eastern Pontides (Ketin, 1966), forms part of the major metallogenic province in Turkey and contains >400 massive and vein-type Cu-Zn-Pb deposits and occurrences (Gökçe and Bozkaya, 2003). The study area in the eastern part of the 'Pontide Tectonic Unit,' contains the following east−west oriented tectonic zones: a volcanic belt, a fore-arc basin fill, a metamorphic complex, an ophiolitic suture zone, and a basin fill (Yılmaz *et al.*, 1997). The study area is on the northern margin of the volcanic belt and the fore-arc basin fill (Figure 1). The Late Cretaceous volcanic belt is dominated by dacitic, andesitic, and partially rhyodacitic and rarely rhyolitic and basaltic lavas and pyroclastics. This belt was followed by Eocene calc-alkaline magmatic rocks which parallel each other (Figure 1). The fore-arc units consist of a Late Cretaceous-Eocene alternating succession of pinkish-gray pyroclastics,

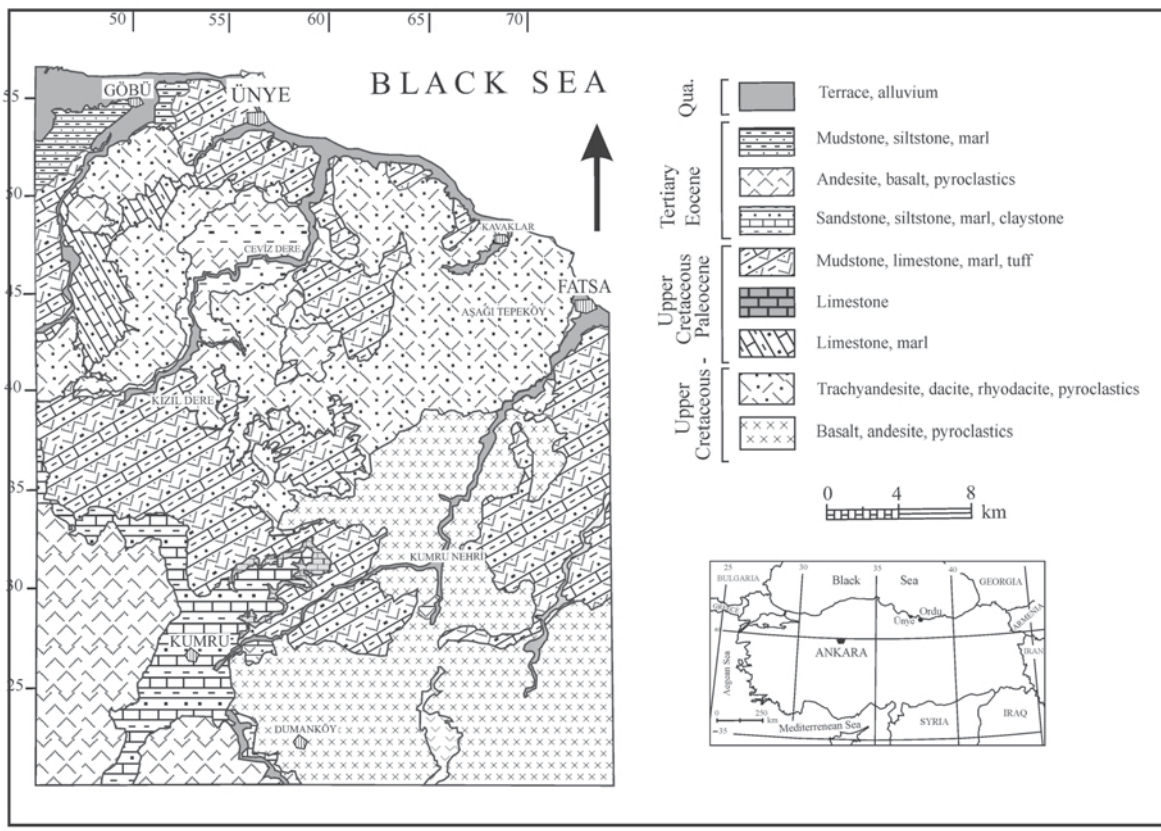

Figure 1. Simplified regional geological and location map of the study area (Keskin *et al.*, 1998).

mudrocks, marls, limestones, sandstones, and conglomerates. The Na-bentonite was formed in a fore-arc basin in an Upper Cretaceous–Paleocene volcano-sedimentary succession. The successions consist mainly of limestone, clayey limestone, pyroclastics (mainly tuff), and conglomerates which pass laterally and vertically into the basement. These rocks are cut by andesitic dykes of Tertiary age and are overlain unconformably by terraces and alluvial deposits (Figure 1). The Ca-bentonites are derived from pyroclastics (mainly tuffs that range from dacitic to rhyodacitic in composition). In the Ca-bentonite deposits, smectite formed within partially preserved pyroclastics, and interfingered with some thin pyroclastics and thin silica lenses. The Ca-bentonite deposits contain no marine fossils or sediments, but the Na-bentonite occasionally contains very thin (0.5−1 cm) limestone and lignite beds or lenses. The Ca-bentonite occurs in a variety of colors including white, yellow, pink, red, yellowish white, and greenish blue and has a mottled, clayey, silty, or sandy texture. The Ca-bentonites have a soapy, 'popcorn' texture and are waxy in appearance. In addition to smectite, unaltered biotites, and altered volcanic rock fragments, opal-CT (cristobalite-tridymite), quartz, and pyrite are commonly observed within the Ca-bentonite. Some parts of the Ca-bentonite show flow textures with remnants of ignimbritic tuff. Perlite lenses and/or nodules are commonly observed within the Ca-bentonite. The alteration of perlite to smectite is extremely irregular. In some places, the perlite is completely unaltered. In others, the alteration is complete, and a huge mass (5−10 m wide) of almost pure bentonite formed. In some areas, the smectite is scattered throughout the glass, or the perlite contains disseminated smectite. Thin, black, fracture-filling aragonite veins occur in the Ca-bentonites. In addition to the aforementioned Ca-bentonite deposits, Ca-bentonites were also deposited in lacustrine sediments, as was Na-bentonite, in the northeast of Ordu area. The Na-bentonites are yellow-greenish or green-white to green-gray in color. They have a soapy, 'popcorn' texture and are waxy in appearance. The Na-bentonite generally contains smaller amounts of non-clay minerals than the Ca-bentonite. Thin silica layers/beds (5−10 cm) have been observed within the Na-bentonite, and silicified tree trunks are present at the base. The most extensive Ca-bentonite deposits are located in nearby Göbü, and the Na-bentonite is located in the Kumru area. The Ca-bentonite ranges from 1 to 30 m thick, and has been exploited from time to time since 1995. using open-pit mining. The Na-bentonite has a similar thickness to the Ca-bentonite but has not been exploited (Figure 1).

MATERIALS AND METHODS

Samples of various rock types were collected from many localities throughout the province and were analyzed by X-ray diffraction (XRD), scanning electron microscopy (SEM) and micro-analysis (SEM) with an energy dispersive system (EDX) for semi-quantitative determination of the mineralogical composition and morphological properties, and inductively coupled plasma mass spectrometry (ICP-MS: ACME Labs, Canada) for trace and *REE* compositions. The mineralogy of the bulk rocks and clay fractions (<2 μm) was determined by means of XRD using randomly oriented specimens. The clay mineralogy was identified from three XRD patterns (air-dried at 25ºC, ethylene-glycolated, and heated at 490ºC for 4 h) of the clay-sized fractions (<2 μm) extracted by gravitational sedimentation technique, followed by centrifugation of the suspension after overnight dispersion in deionized water. Oriented preparations of the clay fractions were obtained by vacuum filtration of the clay suspension and transferred to glass plates. The size and form of submicroscopic clay minerals and their interrelations with other minerals were determined by SEM equipped with EDS (Leo 1430 VT and JSM 6400 model), operating at 20 kV. The total abundances of the major oxides and minor elements were obtained from fusion of 0.1 g samples using Li-metaborate/tetraborate and subsequent digestion with nitric acid by ICP-emission spectrometry. Loss on ignition (LOI) was determined by weight difference after ignition at 1000ºC. Total carbon and sulfur analyses were made by Leco (ACME Laboratories, Canada). Rare earth and refractory elements were determined by ICP-MS following a Li-metaborate/tetraborate fusion and dilute nitric acid digestion. In addition, a separate 0.5 g split of each sample was digested in Aqua Regia and analyzed by ICP-MS for precious and base metals. The detection limit for all major oxides was 0.01 wt.%, except for Fe_2O_3 which was 0.04%; the LOI detection limit was 0.1%. The detection limits (in ppm) for trace metals were: 0.1 for Cs, Hf, Mo, Nb, Ni, Pb, Rb, Sb, Ta, U, Zr, La, and Ce; 0.2 for Co and Th; 0.5 for Ga, Sr, and W; 1.0 for As, Ba, Be, Sn, and Zn; 8.0 for V; 0.01 for Tb, Tm, and Lu; 0.02 for Pr, Eu, and Ho; 0.03 for Er; 0.05 for Sm, Gd, Dy, and Yb; and 0.3 for Nd (Table 1).

The major oxides and most of the trace elements were mobile during the alteration processes of the parent rock in the study area. In addition, all studied samples were classified into three groups according to the mineral paragenesis, chemical composition, and loss on ignition. Two different rocks were accepted as parent rocks. Slightly altered dacite (PR1) was chosen for moderately altered rock (MPR) and Na-bentonites, and perlite (PR2) for Ca-bentonites. Mass-balance calculations were carried out according to MacLean and Kranidiotis (1987). The reconstructed composition of the altered sample was calculated at a constant concentration of the immobile element. This value was computed for each element using MacLean's (1990) equation. In the present study, Zr-Hf in the MPR and Na-bentonite and Er-Y in the Ca-bentonite displayed linear relations when plotted *vs.* each other and

Table 1. Major (wt.%), trace, and rare earth elements (ppm) and chondrite-normalized ratios of some investigated samples.

Sample	PR1	Moderately altered parent rocks					—— Na-bentonites ——				PR2	—— Ca-bentonites ——										STD	DL
Element		MA-1	MA-2	MA-3	MA-4	MA-5	HO-1	HO-2	HO-4	S-14		S-1A	S-3	S-6A	S-6B	S-7	S-8A	S-8B	S-9A	S-10	S-11	S-12		
SiO_2	64.8	67.4	66.3	70.1	50.4	64.7	64.0	59.2	58.1	60.0	73.18	67.4	68.9	68.3	68.4	68.4	66.6	70.7	64.6	66.2	65.2	68.0	58.1	0.01
Al_2O_3	15.0	13.6	13.6	14.3	20.3	16.2	17.9	16.0	16.6	15.9	11.74	12.4	11.5	12.6	13.0	11.8	13.9	11.1	13.1	14.6	13.4	12.9	14.1	0.01
Fe_2O_3	5.1	3.3	4.0	2.7	7.8	2.3	3.9	4.0	4.1	1.3	0.91	1.1	0.9	1.6	1.0	1.2	1.8	1.2	1.2	1.2	1.2	0.9	7.6	0.04
MgO	2.8	1.6	3.2	1.9	5.1	1.4	1.6	3.0	3.6	3.7	0.22	2.1	2.0	1.8	2.3	3.0	1.7	1.8	3.2	2.3	3.1	2.2	3.3	0.01
CaO	1.2	2.1	1.4	0.6	4.4	1.8	2.2	3.5	2.5	1.1	0.42	1.7	1.4	1.3	1.4	1.3	2.2	1.9	1.8	1.2	1.5	1.4	6.4	0.01
Na_2O	4.4	2.7	2.5	4.5	6.0	2.3	2.7	2.2	2.4	2.2	3.39	0.7	0.4	1.0	0.7	0.6	1.4	0.6	0.4	1.8	0.4	0.6	3.7	0.01
K_2O	3.3	2.0	2.8	1.1	0.3	5.6	1.4	0.6	0.6	1.0	3.84	0.6	0.6	2.3	1.5	1.1	2.3	1.3	0.8	2.4	1.0	1.3	2.2	0.01
TiO_2	0.6	0.4	0.5	0.3	0.5	0.3	0.4	0.4	0.4	0.4	0.08	0.1	0.1	0.1	0.1	0.1	0.2	0.1	0.1	0.1	0.1	0.1	0.7	0.01
P_2O_5	0.12	0.08	0.11	0.06	0.14	0.09	0.12	0.14	0.14	0.11	<0.01	0.001	0.001	0.001	0.001	0.02	0.03	0.001	0.001	0.02	0.02	0.02	0.8	0.01
MnO	0.1	0.0	0.2	0.1	0.1	0.2	0.1	0.1	0.1	0.2	0.06	0.0	0.0	0.0	0.0	0.0	0.0	0.0	0.1	0.0	0.0	0.0	0.4	0.01
LOI	2.4	6.6	5.3	4.2	4.7	6.0	5.4	10.7	11.2	14.4	6.1	13.9	14.1	10.9	11.5	12.5	9.8	11.2	14.6	10.1	14.0	12.5	1.9	0.10
Sum	99.8	99.8	99.9	99.9	99.7	99.9	99.9	99.8	99.8	99.8	99.93	99.9	99.9	99.9	99.9	99.9	99.9	99.9	99.9	99.9	99.9	99.9	99.70	
Ba	623.0	187.6	154.5	207.8	98.8	169.0	462.0	473.0	499.0	255.0	12	17.0	16.0	10.0	56.0	9.0	86.0	40.0	36.0	21.0	31.0	20.0	497	1.00
Be	3.0	1.0	1.0	1.0	1.0	3.0	<1	3.0	3.0	8.0	7	6.0	8.0	6.0	7.0	6.0	12.0	7.0	11.0	7.0	7.0	6.0	1.0	0.20
Co	12.3	4.4	4.5	5.0	23.7	1.1	1.1	7.6	6.8	1.7	9.8	1.8	2.0	7.7	5.6	7.6	4.0	2.7	2.3	3.8	4.1	5.7	27.2	0.10
Cs	2.2	1.6	0.8	0.3	0.1	0.9	1.0	2.2	2.4	1.6	5.0	3.0	4.4	4.5	5.6	2.6	4.7	3.7	2.4	1.4	3.8	4.7	6.9	0.50
Ga	16.4	13.1	13.5	14.0	18.8	13.9	16.4	13.4	13.7	18.6	13.7	14.2	13.9	14.7	14.6	14.0	14.8	12.0	14.4	16.6	15.5	14.5	17.2	0.10
Hf	4.5	3.2	2.6	4.8	2.8	6.1	5.1	3.2	3.2	6.3	4.5	4.5	4.5	5.1	4.9	4.6	4.4	4.6	5.8	5.8	5.4	5.0	9.6	0.10
Nb	11.0	4.9	4.3	6.0	3.9	11.9	11.8	10.4	9.9	10.2	53.7	49.5	49.1	64.9	49.5	48.2	69.3	44.8	50.6	47.0	46.9	46.1	21.2	0.10
Rb	118.6	40.1	36.4	29.8	2.5	79.2	114.9	41.4	41.6	35.4	220.6	25.1	40.4	142.3	133.7	63.7	124.6	83.2	34.0	37.7	89.6	103.8	28.2	0.10
Sc	15.0	9.0	10.0	10.0	8.0	7.0	3.0	8.0	7.0	8.0	<1.0	13.9	1.8	10.9	11.5	12.5	9.8	11.2	14.6	10.1	14.0	12.5	25	0.50
Sn	4.0	1.0	1.0	1.0	1.0	2.0	1.0	1.0	1.0	4.0	3	3.0	6.0	3.0	3.0	3.0	2.0	2.0	3.0	4.0	4.0	4.0	15	0.10
Sr	147.4	136.2	34.5	139.4	419.1	161.8	155.8	481.6	478.9	221.5	16.2	182.3	170.2	196.1	232.2	147.8	258.1	262.3	152.8	87.1	119.1	208.2	406.8	0.20
Ta	0.7	0.4	0.3	0.5	0.4	1.2	0.8	0.6	0.7	5.3	4.7	4.5	4.6	4.9	4.9	4.6	3.4	3.4	4.6	4.7	5.1	4.9	7.2	0.10
Th	10.7	3.2	2.5	5.0	5.4	30.8	9.1	8.6	9.3	10.0	27.0	23.0	26.8	26.6	26.0	25.6	24.1	19.0	24.5	26.4	28.7	24.8	10.3	8.00
U	3.5	0.8	0.9	1.5	0.2	2.7	3.7	2.8	2.5	0.8	9.1	4.3	2.0	2.3	0.6	2.2	1.4	0.5	0.3	2.7	8.6	0.6	16.4	0.50
V	97.0	38.0	44.0	34.0	102.0	11.0	37.0	71.0	58.0	16.0	<8	4.0	3.0	2.0	3.0	2.0	13.0	12.0	2.0	3.0	9.0	4.0	207	0.10
W	2.1	0.5	0.3	1.2	0.9	2.1	2.5	5.8	5.5	3.5	61.7	9.4	15.9	42.8	30.8	42.6	15.3	8.4	8.9	22.8	14.9	43.1	14.8	0.10
Zr	159.4	111.0	95.9	164.5	108.3	198.9	170.7	121.2	119.9	178.6	111.2	120.2	114.0	130.1	136.3	142.8	130.1	133.5	159.1	123.2	142.7	129.7	284.9	0.10
Mo	1.2	0.5	0.4	0.5	0.2	0.1	<0.1	0.2	0.2	0.3	1.4	0.2	2.8	0.6	0.2	0.2	0.2	0.2	<0.1	0.3	<0.1	0.2	19.1	1.00
Cu	23.1	5.5	1.3	2.7	1.4	2.8	14.0	19.1	10.9	6.6	0.9	1.0	1.5	1.6	0.6	1.0	2.1	2.3	1.4	1.5	2.6	1.2	106.9	0.10
Pb	15.9	7.5	4.2	3.0	1.0	9.4	5.4	10.3	6.1	14.9	1.6	9.8	3.7	9.2	7.1	7.8	9.0	6.6	9.7	4.6	6.1	8.5	65.9	0.10
Zn	67.0	45.0	81.0	40.0	51.0	21.0	10.0	14.0	11.0	18.0	5.0	10.0	2.0	13.0	13.0	19.0	15.0	16.0	22.0	13.0	16.0	12.0	385	0.10
Ni	20.0	3.5	0.7	2.0	17.6	1.0	0.2	0.5	<0.1	0.7	1.1	0.6	1.6	2.9	3.3	3.2	2.8	2.3	2.2	2.0	2.6	2.8	53.2	0.10
As	8.6	2.3	0.5	28.0	0.5	1.1	2.0	<0.5	<0.5	6.1	0.6	5.7	1.8	<0.5	0.8	0.7	3.2	1.6	1.9	1.3	5.5	<0.5	53.4	0.02
Y	23.4	22.7	23.1	27.7	11.7	24.1	7.0	17.1	19.2	29.2	25.6	24.1	23.3	18.9	15.6	32.4	24.6	19.5	27.6	23.8	29.5	14.5	31.5	0.30
La	30.6	13.4	12.2	13.0	14.8	57.5	24.1	24.5	26.7	22.3	37.7	34.8	42.4	46.6	37.4	67.2	65.7	39.7	44.6	43.3	46.9	37.5	12.1	0.05
Ce	62.6	26.3	23.9	26.3	27.9	68.4	36.3	48.9	53.9	104.8	68.6	62.4	68.6	63.9	45.0	78.7	96.4	56.5	90.5	71.1	47.0	50.0	27.3	0.02
Pr	7.1	3.0	2.7	2.9	2.9	10.1	2.8	5.3	6.1	7.2	6.68	6.2	7.3	7.1	4.7	11.4	10.8	6.2	7.2	7.1	7.7	5.1	3.41	0.05
Nd	26.4	12.8	12.4	12.7	11.0	33.1	7.4	21.0	24.2	21.8	20.6	19.9	23.3	20.9	14.1	35.6	35.0	19.8	22.6	22.0	22.4	14.4	13.9	0.01

Sm	4.7	2.8	2.8	2.8	2.5	5.0	0.9	3.5	4.1	3.7	3.55	3.4	3.6	3.2	2.0	5.8	5.5	3.1	3.9	3.5	3.3	2.0	2.91	0.05
Eu	1.0	0.8	0.9	0.6	1.8	1.0	0.2	1.0	1.2	0.2	0.10	0.10	0.10	0.10	0.10	0.20	0.40	0.20	0.20	0.10	0.10	0.10	0.86	0.02
Gd	4.3	2.9	3.0	3.1	2.2	3.8	0.7	3.1	3.4	3.1	3.09	3.1	3.1	2.6	1.7	4.7	4.2	2.7	3.4	3.1	2.9	1.6	2.91	0.03
Tb	0.7	0.5	0.6	0.6	0.4	0.7	0.1	0.5	0.6	0.6	0.61	0.6	0.6	0.5	0.3	0.9	0.7	0.5	0.7	0.6	0.6	0.3	0.51	0.01
Dy	3.8	3.2	3.5	4.0	2.2	4.1	0.9	2.7	3.1	4.1	3.71	3.6	3.5	2.8	2.1	5.0	4.1	2.9	4.0	3.7	3.8	2.0	2.98	0.05
Ho	0.8	0.7	0.8	0.9	0.4	0.8	0.2	0.6	0.7	0.9	0.83	0.8	0.7	0.6	0.5	1.1	0.8	0.6	0.9	0.8	0.8	0.4	0.61	0.01
Er	2.2	2.3	2.4	3.0	1.2	2.5	0.8	1.7	2.0	3.1	2.68	2.6	2.4	1.9	1.6	3.5	2.5	2.0	3.0	2.5	2.8	1.5	1.84	0.03
Tm	0.4	0.4	0.4	0.5	0.2	0.4	0.2	0.3	0.3	0.5	0.48	0.4	0.4	0.3	0.3	0.6	0.4	0.4	0.5	0.4	0.5	0.3	0.28	0.01
Yb	2.2	2.6	2.5	3.1	1.2	2.8	1.2	1.9	2.1	3.9	3.28	3.0	3.0	2.3	2.3	4.0	2.9	2.5	3.8	3.0	3.1	2.0	1.77	0.05
Lu	0.3	0.4	0.4	0.5	0.2	0.5	0.2	0.3	0.3	0.6	0.52	0.5	0.5	0.4	0.4	0.6	0.5	0.4	0.6	0.5	0.5	0.3	0.27	0.01
REE	147.0	72.1	68.4	73.9	68.8	190.7	75.8	115.2	128.7	176.8	152.0	141.4	159.5	153.0	112.4	219.1	229.8	137.3	185.9	161.6	142.3	117.3		
LRE	126.7	55.5	51.2	54.9	56.6	169.1	70.6	99.7	110.9	156.1	133.4	123.3	141.6	138.5	101.2	192.9	207.9	122.2	164.9	143.5	124.0	107.0		
MRE	15.2	10.9	11.6	11.9	9.5	15.4	2.9	11.4	13.0	12.6	11.9	11.6	11.6	9.6	6.6	17.6	15.7	9.9	13.0	11.7	11.6	6.3		
HREE	5.1	5.7	5.7	7.1	2.7	6.2	2.3	4.1	4.8	8.2	7.0	6.5	6.3	4.9	4.6	8.6	6.2	5.2	8.0	6.4	6.8	4.0		
LILE	16770	23432	9807	2977	47319	28243	11919	6072	6099	5672	32272	5019	19177	13323	9617	19345	11134	6951	19887	8762	11163	28019		
TRE	105.4	141.5	93.7	203.7	43.9	219.4	64.2	120.2	93.7	13.4	16.8	7.1	25.2	22.5	30.8	36.9	35.3	27.9	20.3	34.3	21.7	18.2		
HFSE	2627	3341	2476	3964	2230	4176	3437	3057	3203	783	180	656	689	680	767	1537	850	884	867	827	753	728		
Eu*	1.02	0.89	1.03	0.61	1.13	0.77	0.77	0.99	1.04	0.89	0.10	0.12	0.09	0.13	0.14	0.10	0.26	0.22	0.21	0.14	0.15	0.15		
Ce*	1.03	0.99	1.01	1.03	1.03	0.68	1.03	1.03	1.02	1.99	1.04	1.02	0.94	0.85	0.81	0.69	0.87	0.87	1.21	0.98	0.60	0.87		
$(La/Sm)_N$	3.01	2.74	2.92	3.72	7.28	4.14	17.60	4.42	4.14	11.13	6.68	6.38	7.39	9.16	11.82	7.30	7.51	8.13	7.25	7.72	8.99	12.04		
$(La/Yb)_N$	3.50	3.33	2.83	8.68	13.70	9.33	13.89	8.69	8.45	3.85	7.75	7.85	9.59	13.66	11.16	11.41	15.49	10.84	7.89	9.73	10.33	12.97		
$(Gd/Yb)_N$	0.80	0.85	0.70	1.36	0.96	1.37	0.41	1.14	1.13	0.13	0.67	0.74	0.74	0.79	0.52	0.84	1.05	0.76	0.63	0.73	0.67	0.57		
$(La/Lu)_N$	9.35	3.48	3.17	2.60	8.54	13.27	13.18	8.21	8.40	3.86	7.53	7.69	9.18	13.45	11.10	11.08	15.17	10.57	7.59	9.78	10.15	12.17		
Rb/La	3.87	2.99	2.98	2.29	0.17	1.38	4.77	1.69	1.56	1.59	5.82	0.72	0.95	3.054	3.57	0.95	1.89	2.10	0.76	0.87	1.91	2.77		
Ba/La	20.4	14.0	12.7	16.0	6.68	2.94	19.2	19.3	18.7	11.43	0.32	0.49	0.38	0.215	1.5	0.13	1.31	1.01	0.81	0.49	0.66	0.53		
K/La	890	1221	1899	722	163	813	465	203	187	376	842	153	110	401	342	137	284	268	147	453	179	286		
Th/La	0.35	0.24	0.21	0.38	0.36	0.54	0.38	0.35	0.35	0.45	0.71	0.66	0.63	0.57	0.70	0.38	0.37	0.48	0.55	0.61	0.61	0.66		

PR1: parent rock (dacite) and PR2: parent rock (perlite).
ΣFe_2O_3: total Fe.
STD: standard for major, trace, and refractory elements are SO-18 and STD DS7, respectively.
DL: Detection limits of major elements and LOI (in %) and trace elements (in ppm).

Table 2. Correlation coefficients of major oxides and some trace elements and element groups in Na-bentonites and Ca-bentonites (shaded).

	SiO_2	Al_2O_3	Fe_2O_3	MgO	CaO	Na_2O	K_2O	TiO_2	P_2O_5	MnO	Hf	Nb	Zr	*REE*	*LREE*	*MREE*	*HREE*	LILE	TRE	HFSE	
SiO_2	**1.00**	***−0.71***	−0.32	***−0.81***	−0.56	*0.55*	*0.51*	−0.30	−0.43	0.04	−0.65	−0.03	−0.61	−0.24	−0.25	−0.17	−0.20	*0.51*	−0.28	−0.62	SiO_2
Al_2O_3	***−0.82***	**1.00**	0.37	0.29	0.20	0.07	0.16	0.40	*0.58*	−0.02	*0.61*	0.25	0.21	0.14	0.16	0.00	−0.06	0.16	0.20	*0.52*	Al_2O_3
Fe_2O_3	−0.64	*0.59*	**1.00**	0.04	0.49	−0.01	0.21	*0.68*	0.37	0.03	0.03	**0.80**	0.23	*0.56*	*0.59*	0.38	0.00	0.22	*0.61*	*0.68*	Fe_2O_3
MgO	***−0.83***	*0.52*	*0.63*	**1.00**	0.47	***−0.80***	***−0.75***	−0.06	0.27	−0.18	*0.55*	−0.34	**0.79**	0.15	0.14	0.15	0.28	***−0.75***	0.33	0.38	MgO
CaO	***−0.81***	**0.70**	**0.80**	*0.53*	**1.00**	−0.65	−0.58	0.70	0.27	−0.23	−0.04	0.20	0.45	0.32	0.34	0.19	−0.05	−0.57	0.48	**0.88**	CaO
Na_2O	−0.34	*0.50*	*0.67*	0.43	0.37	**1.00**	**0.93**	0.05	−0.03	0.44	−0.13	0.27	−0.56	0.07	0.07	0.11	0.10	**0.93**	−0.19	−0.38	Na_2O
K_2O	0.45	−0.31	−0.53	−0.56	−0.36	−0.36	**1.00**	0.11	0.06	0.33	−0.08	0.44	−0.43	0.07	0.08	0.01	−0.09	**1.00**	0.03	−0.26	K_2O
TiO_2	−0.63	*0.54*	**0.88**	**0.74**	*0.60*	0.49	−0.62	**1.00**	0.49	0.07	−0.17	*0.60*	0.11	*0.60*	*0.62*	0.43	0.08	0.12	*0.51*	**0.86**	TiO_2
P_2O_5	***−0.78***	**0.72**	*0.57*	*0.58*	*0.65*	0.01	−0.41	**0.71**	**1.00**	−0.26	0.10	0.17	0.16	0.47	0.49	0.38	0.11	0.06	0.49	*0.63*	P_2O_5
MnO	−0.30	0.16	−0.23	0.41	−0.15	−0.24	0.30	0.08	0.27	**1.00**	0.13	0.19	0.21	0.24	0.22	0.31	*0.53*	0.33	0.06	−0.25	MnO
Hf	0.27	0.03	***−0.75***	−0.42	−0.55	−0.26	0.39	−0.62	−0.28	0.36	**1.00**	−0.24	*0.52*	−0.12	−0.12	−0.17	0.09	−0.08	0.14	0.04	Hf
Nb	−0.02	0.19	−0.53	−0.35	−0.10	−0.61	0.22	−0.46	0.25	0.22	*0.65*	**1.00**	−0.10	0.49	*0.53*	0.28	−0.07	0.45	0.23	0.41	Nb
Zr	0.28	0.09	−0.70	−0.49	−0.49	−0.20	0.43	−0.65	−0.28	0.25	**0.98**	0.69	**1.00**	0.24	0.24	0.16	0.28	−0.42	*0.66*	0.35	Zr
REE	−0.12	0.04	−0.66	−0.07	−0.21	−0.52	0.44	−0.60	−0.03	*0.58*	*0.68*	**0.70**	*0.64*	**1.00**	**1.00**	**0.93**	*0.69*	0.07	0.38	*0.53*	*REE*
LREE	−0.15	0.10	−0.63	−0.07	−0.17	−0.52	0.42	−0.56	0.03	*0.58*	0.69	**0.75**	*0.66*	**1.00**	**1.00**	**0.90**	*0.64*	0.09	0.39	*0.56*	*LREE*
MREE	0.13	−0.44	−0.48	0.01	−0.29	−0.27	0.43	−0.59	−0.47	0.29	0.13	0.01	0.10	*0.61*	*0.54*	**1.00**	**0.86**	0.01	0.29	0.35	*MREE*
HREE	0.48	−0.66	***−0.77***	−0.18	***−0.77***	−0.30	0.30	−0.64	***−0.71***	0.31	0.47	−0.02	0.35	0.49	0.42	**0.73**	1.00	−0.10	0.10	0.00	*HREE*
LILE	0.44	−0.30	−0.53	−0.56	−0.35	−0.37	**1.00**	−0.62	−0.40	0.30	0.39	0.24	0.43	0.45	0.43	0.43	0.29	**1.00**	0.03	−0.26	LILE
TRE	−0.45	0.29	**0.91**	*0.58*	*0.67*	*0.66*	−0.38	**0.74**	0.27	−0.22	***−0.86***	***−0.75***	***−0.81***	−0.69	−0.70	−0.21	−0.53	−0.39	**1.00**	*0.57*	TRE
HFSE	***−0.71***	*0.64*	**0.84**	**0.74**	*0.64*	0.41	−0.60	**0.98**	**0.83**	0.16	−0.52	−0.28	−0.55	−0.47	−0.42	−0.61	−0.69	−0.60	*0.64*	**1.00**	HFSE
	SiO_2	Al_2O_3	Fe_2O_3	MgO	CaO	Na_2O	K_2O	TiO_2	P_2O_5	MnO	Hf	Nb	Zr	*REE*	*LREE*	*MREE*	*HREE*	LILE	TRE	HFSE	

Bold, italic, and bold-italic characters indicate strongly positive, moderately positive, and strongly negative correlation coefficients, respectively.

showed the large positive correlation coefficients (r = 0.95; r = 0.98), and straight lines of regression pass through the origin. The compositions of the parent rocks were plotted on the same inclinations because the ratios of these elements to each other in bentonites are very similar to those of the parent rocks, as indicated by MacLean (1990) (Table 2). Zr for MPR and Na-bentonite and Er for Ca-bentonite were used as immobile elements for the mass-balance calculation in the above-mentioned equation of MacLean (1990)

$$C_e = [(E_a/IM_a) \times IM_p] - E_p \quad (1)$$

where C_e is the computed element wt.%, E_a and E_p are the concentrations of the computed element in the altered and parent rock, respectively, and IM_a and IM_p are the concentrations of immobile elements in the altered and parent rocks, respectively. Mass gains and losses of components are equivalent to weight percent changes if the precursor mass is taken as 100 g.

Using the equation, loss and/or gains of all major and trace elements were computed and some were shown with total rare-earth elements (*REE*, *LREE*, *HREE*), high field-strength elements (HFSE, *e.g.* Hf, Nb, Ta, Ti, Zr, and P (Saunders *et al.*, 1980)), large-ion lithophile

Figure 2. Mass balance change of the major (g), trace (ppm), and total TRE, *REE*, HFSE, and LILE (ppm) elements of the investigated samples. Mass gains and losses of components are equivalent to wt.% changes if the precursor mass is taken as 100 g.

Table 3. Mass gains and losses of the moderately altered rocks (MPR), and of Na-bentonite and Ca-bentonite samples (mass gains and losses of components are equivalent to wt.% changes if the precursor mass is taken as 100 g with constant Zr for MPR and Na-bentonites and constant Er for Ca-bentonites).

Element	Moderately altered rocks					Na-bentonites				Ca-bentonites									
	MA-1	MA-2	MA-3	MA-4	MA-5	HO-1	HO-2	HO-4	S-14	S-1A	S-3	S-6A	S-6B	S-7	S-8A	S-8B	S-9A	S-10	S-11	S-12
g																				
SiO_2	32.0	45.5	3.7	9.4	−12.9	−5.0	13.1	12.5	−11.3	−4.3	3.5	23.6	39.3	−20.0	−1.1	22.6	−15.5	−2.2	−10.5	50.9
Al_2O_3	4.5	7.6	−1.1	14.8	−2.0	1.7	6.0	7.0	−0.8	1.1	1.1	6.1	9.7	−2.6	3.3	3.3	0.0	3.9	1.1	11.8
Fe_2O_3	−0.3	1.6	−2.5	6.3	−4.1	−1.4	0.2	0.4	−4.0	0.2	0.1	1.4	0.7	0.0	1.0	0.7	0.1	0.4	0.2	0.7
MgO	−0.5	2.6	−0.9	4.8	−1.6	−1.3	1.2	2.0	0.5	2.0	2.0	2.4	3.6	2.1	1.6	2.3	2.6	2.2	2.7	3.8
CaO	1.9	1.2	−0.6	5.4	0.3	0.9	3.4	2.2	−0.2	1.4	1.2	1.4	1.8	0.6	2.0	2.1	1.2	0.9	1.0	2.1
Na_2O	−0.5	−0.3	0.0	4.4	−2.6	−1.8	−1.6	−1.2	−2.4	−2.9	−2.9	−2.0	−2.3	−3.0	−1.9	−2.6	−3.0	−1.4	−3.0	−2.3
K_2O	−0.5	1.4	−2.2	−2.9	1.2	−2.0	−2.5	−2.5	−2.4	−3.4	−3.2	−0.6	−1.3	−3.0	−1.4	−2.1	−3.1	−1.3	−2.9	−1.5
TiO_2	−0.1	0.2	−0.3	0.2	−0.4	−0.2	−0.1	0.0	−0.2	0.0	0.0	0.0	0.1	0.0	0.1	0.1	0.0	0.0	0.0	0.1
MnO	0.0	0.2	0.0	0.1	0.0	0.0	0.0	0.0	0.1	0.0	−0.1	0.0	0.0	0.0	0.0	0.0	0.0	0.0	0.0	0.0
ppm																				
Ba	−354	−366	−422	−478	−488	−192	−0.9	40.4	−395	5.5	5.8	2.2	80.1	−5.0	80.9	42.1	20.2	10.5	17.8	24.5
Co	−6.0	−4.8	−7.5	22.6	−11.4	−12.3	−2.3	−3.3	−10.8	−8.0	−7.6	1.1	−0.6	−3.9	−5.5	−6.1	−7.7	−5.7	−5.9	0.6
Cs	0.1	−0.9	−1.9	−2.1	−1.5	−1.3	0.7	1.0	−0.8	−1.9	−0.1	1.4	4.2	−3.0	0.1	0.0	−2.9	−3.5	−1.3	3.6
Ga	2.4	6.0	−2.8	11.3	−5.3	−1.1	1.2	1.8	0.2	0.9	1.8	7.1	10.3	−2.8	2.3	2.5	−0.8	4.1	1.2	12.7
Hf	0.1	−0.2	0.2	−0.4	0.4	0.3	−0.3	−0.2	1.1	0.1	0.5	2.7	3.6	−0.9	0.3	1.7	0.7	1.7	0.7	4.6
Nb	−4.0	−3.9	−5.2	−5.3	−1.5	0.0	2.7	2.2	−1.9	−2.9	0.9	38.3	27.7	−16.3	21.2	6.9	−8.5	−3.3	−8.6	30.3
Rb	−61.0	−58.1	−89.7	−114.9	−55.1	−11.3	−64.2	−63.3	−87.0	−194.8	−176	−18.8	−0.8	−171	−86.0	−108.0	−190.2	−180.2	−134.5	−31.4
Sr	48.2	−90.1	−12.3	469.4	−17.7	−95.3	486.0	489.3	50.3	171.0	173.1	261.9	365.6	98.6	262.7	338.8	120.3	77.2	98.2	363.4
Ta	−0.1	−0.2	−0.2	−0.1	0.3	0.0	0.1	0.2	4.0	−0.1	0.4	2.2	3.4	−1.1	−1.0	−0.1	−0.6	0.3	0.2	4.2
Th	−6.1	−6.5	−5.9	−2.8	14.0	−2.2	0.6	1.7	−1.8	−3.4	2.8	10.7	15.7	−7.1	−1.0	−1.3	−5.1	1.3	0.6	18.2
U	−2.4	−2.0	−2.0	−3.2	−1.3	0.0	0.2	−0.2	−2.8	−4.7	−6.9	−5.8	−8.1	−7.4	−7.6	−8.4	−8.8	−6.2	−0.8	−8.0
W	−1.4	−1.6	−0.9	−0.8	−0.4	0.2	5.5	5.2	1.0	−52.0	−44.0	−1.0	−11.1	−28.6	−45.2	−50.3	−53.7	−37.3	−47.4	16.9
Zr	0.0	0.0	0.0	0.0	0.0	0.0	0.0	0.0	0.0	12.2	15.6	73.3	112.9	−0.3	29.4	69.5	30.9	20.9	25.9	125.3
Mo	−0.5	−0.5	−0.7	−0.9	−1.1	0.0	−0.9	−0.9	−0.9	−1.2	1.7	−0.5	−1.1	−1.2	−1.2	−1.1	–	−1.1	–	−1.0
Cu	−15.2	−20.9	−20.5	−21.0	−20.9	−10.0	2.0	−8.6	−17.2	0.1	0.8	1.4	0.1	−0.1	1.4	2.2	0.4	0.7	1.6	1.3
Pb	−5.1	−8.9	−13.0	−14.4	−8.4	−10.9	−2.4	−7.8	−2.6	8.5	2.5	11.4	10.1	4.5	8.1	7.3	7.1	3.3	4.3	13.9
Zn	−2.4	67.6	−28.2	8.1	−50.2	−57.7	−48.6	−52.4	−50.9	5.3	−2.8	13.4	16.4	9.8	11.2	16.7	14.7	8.9	10.4	16.9
Ni	−15.0	−18.8	−18.1	5.9	−19.2	−19.8	−19.3	−20.0	−19.4	−0.5	0.7	3.0	4.3	1.4	1.9	2.0	0.9	1.0	1.4	4.0
As	−5.3	−7.8	18.5	−7.9	−7.7	−6.7	0.0	0.0	−3.2	5.3	1.4	–	0.7	−0.1	2.9	1.6	1.1	0.8	4.7	–
Y	9.2	15.0	3.4	−6.2	−4.1	−16.9	−0.9	2.1	2.7	−0.9	0.3	1.2	0.0	−0.4	1.0	0.8	−0.9	−0.1	2.7	0.8
La	−11.4	−10.3	−18.0	−8.8	15.5	−8.1	1.6	4.9	−10.7	−2.0	9.5	28.4	23.8	14.5	33.3	16.0	2.1	8.7	7.4	30.7
Ce	−24.8	−22.9	−37.1	−21.5	−7.8	−28.7	1.7	9.1	30.9	−4.5	7.7	22.0	5.4	−7.5	35.6	7.9	12.2	7.6	−23.5	22.6
Pr	−2.7	−2.7	−4.2	−2.9	1.1	−4.4	0.0	1.0	−0.6	−0.3	1.4	3.4	1.1	2.1	5.0	1.7	−0.2	0.9	0.7	2.5
Nd	−8.0	−5.8	−14.1	−10.2	0.1	−19.5	1.2	5.8	−6.9	−0.2	5.3	9.0	2.6	7.1	17.2	6.2	−0.4	3.0	0.9	5.7
Sm	−0.6	0.0	−1.9	−1.0	−0.7	−3.8	−0.1	0.7	−3.5	0.0	0.5	1.0	−0.3	0.9	2.4	0.6	−0.1	0.2	−0.4	0.0
Eu	−0.3	0.1	−0.9	−0.2	−0.6	−1.2	−0.1	0.2	−1.2	0.0	0.0	0.1	0.0	0.0	0.3	0.2	0.1	0.1	0.0	0.0
Gd	−0.1	0.6	−1.3	−1.0	−1.2	−3.6	−0.2	0.3	−3.6	0.1	0.4	0.5	−0.4	0.6	1.5	0.5	−0.1	0.2	−0.3	−0.2
Tb	0.1	0.2	−0.1	−0.2	−0.2	−0.6	−0.1	0.1	−0.1	0.0	0.0	0.0	−0.1	0.1	0.1	0.0	0.0	0.0	−0.1	0.0

Dy	0.7	2.0	0.0	−0.6	−0.6	−3.0	−0.2	0.3	−0.2	0.0	0.2	0.2	−0.2	0.2	0.7	0.2	−0.1	0.2	−0.1	−0.1		
Ho	0.3	0.5	0.1	−0.2	−0.1	−0.6	0.0	0.1	0.0	0.0	−0.1	−0.3	−0.4	0.2	−0.5	−0.4	−0.2	−0.2	−0.1	−0.4		
Er	1.1	1.8	0.7	−0.4	−0.2	−1.5	0.0	0.4	0.6	−0.6	−0.3	−0.8	−1.1	0.8	−1.7	−1.2	−0.5	−0.7	−0.2	−1.2		
Tm	0.2	0.3	0.1	−0.1	0.0	−0.2	0.0	0.1	0.1	0.0	0.0	0.0	0.0	0.0	0.0	0.0	0.0	0.0	0.0	0.0		
Yb	1.5	1.9	0.8	−0.5	0.1	−1.1	0.3	0.6	1.3	−0.2	0.0	0.0	0.4	−0.2	−0.2	0.1	0.1	−0.1	−0.3	0.3		
Lu	0.2	0.3	0.2	−0.1	0.0	−0.2	0.1	0.1	0.2	0.0	0.0	0.0	0.1	0.0	0.0	0.0	0.0	0.0	−0.1	0.1		
REE	−43.8	−33.8	−75.8	−47.6	5.4	−76.6	4.1	23.6	10.4	−7.2	25.0	64.5	32.4	17.8	95.9	33.5	13.7	20.8	−15.7	61.4		
LREE	−46.9	−41.6	−73.4	−43.4	8.9	−60.7	4.5	20.7	12.7	−7.0	23.9	62.8	32.9	16.2	91.1	31.8	13.8	20.2	−14.5	61.4		
MREE	0.1	3.6	−4.1	−3.1	−3.3	−12.9	−0.7	1.7	−4.4	0.1	1.0	1.8	−1.0	1.8	5.0	1.5	−0.2	0.7	−0.8	−0.4		
HREE	3.0	4.3	1.7	−1.1	−0.2	−3.0	0.3	1.2	2.2	−0.3	0.0	−0.1	0.5	−0.2	−0.2	0.1	0.2	−0.1	−0.4	0.4		
LILE	−4160	10704	−18740	−23861	9679	−17113	−20257	−20134	−20166	−26448	−26691	−5080	−10367	−24802	−11368	−17202	−26063	−10954	−23856	−11921		
TRE	−68.0	15.8	−128.6	80.4	−184.2	−159.4	−61.3	−94.8	−195.3	−3.0	−8.9	18.9	20.2	7.1	23.1	31.0	8.1	5.0	16.1	22.8		
HFSE	−404	1376.6	−1777	1657.5	−2390	−966.8	−155.8	81.3	−1536	623.5	549.6	796.8	937.2	415.8	1481	970.6	609.5	749.8	614.2	1192		

elements (LILE, *e.g.* Ba, K, Rb, Sr, Th, U, Pb, La, and Ce (Schilling, 1973)), and transition elements (TRE, *e.g.* Co, Cr, Cu, Ni, V, Sc, and Zn (Jenner, 1996)) as presented here (Figure 2, Table 3).

RESULTS

Petrography and mineralogy of the rocks and bentonites

The PR1 and moderately altered (MPR) samples are gray to dark gray in color. The dacite PR1 and MPR (MA-1−MA-4) and rhyodacite (MA-5) consist of small phenocrysts (0.1−3.0 mm) of quartz (4−8%), zoned and twinned plagioclase feldspar (30−40%), and locally of sanidine, hornblende (2−4%), biotite (5−10%), sparse pyroxene (1−3%), and opaque minerals (0−1%) in a glassy microcrystalline groundmass (40−55%). The predominant textures are microlithic porphyry, hyalomicrolithic porphyry, glomeroporphyritic, and aphanitic. Plagioclase phenocrysts have the smallest anorthite contents in the dacite (PR1, MA-1−MA-4) (An_{30}−An_{35}) and rhyodacite (An_{18}−An_{24}). Subhedral to euhedral plagioclases are the most common phenocryst phase and these crystals are sometimes >1 mm long. The plagioclase phenocrysts often show normal or oscillatory zoning. Two types of plagioclase are found together. The first is quite clear and characterized by normal zoning. The second is marked by a sieve or dusty texture in the core or rim. Euhedral to subhedral phenocrysts of quartz are strongly corroded and embayed. Biotite and hornblende are partially oxidized and were converted to omphacite pseudomorphs in some cases. The groundmass is typically glassy (colorless, variably devitrified) and locally flow-banded with fine-grained plagioclase crystallites (Figure 3).

The alteration propagates from the fractures to the massive glass. In a volcanic groundmass dominated by microcrystalline quartz and rare Fe-bearing fractures, argillized, sericitized sanidine and plagioclase phenocrysts occur and biotite and hornblende converted rarely to Fe oxides. In spite of the intense argillization, the structure of the pumice components was partially preserved from alteration.

Late Cretaceous dacitic and perlitic volcanic rocks were altered to various secondary minerals, including opal-CT, kaolinite, smectite (mainly montmorillonite), illite, quartz, alunite, pyrite, and gypsum. Original fragments of the volcanoclastic material, which are generally volcanic glass, were altered intensely to Ca- and Na-montmorillonite in the study area. Bentonite deposits contain ~0−10% non-clay minerals, including biotite, opal-CT, cristobalite, and pyrite. Bentonite deposits are observed in the vicinity of the Fatsa, Ünye, Göbü, Kumru, and Ulubey districts (Ordu) (Figure 1). The sizes of these altered hyaloclasts range from coarse lutite through arenite, with lapilli up to 1−3 mm long.

Mineralogically, the Göbü bentonite deposits are partly homogeneous and consist mainly of Ca-montmorillonite

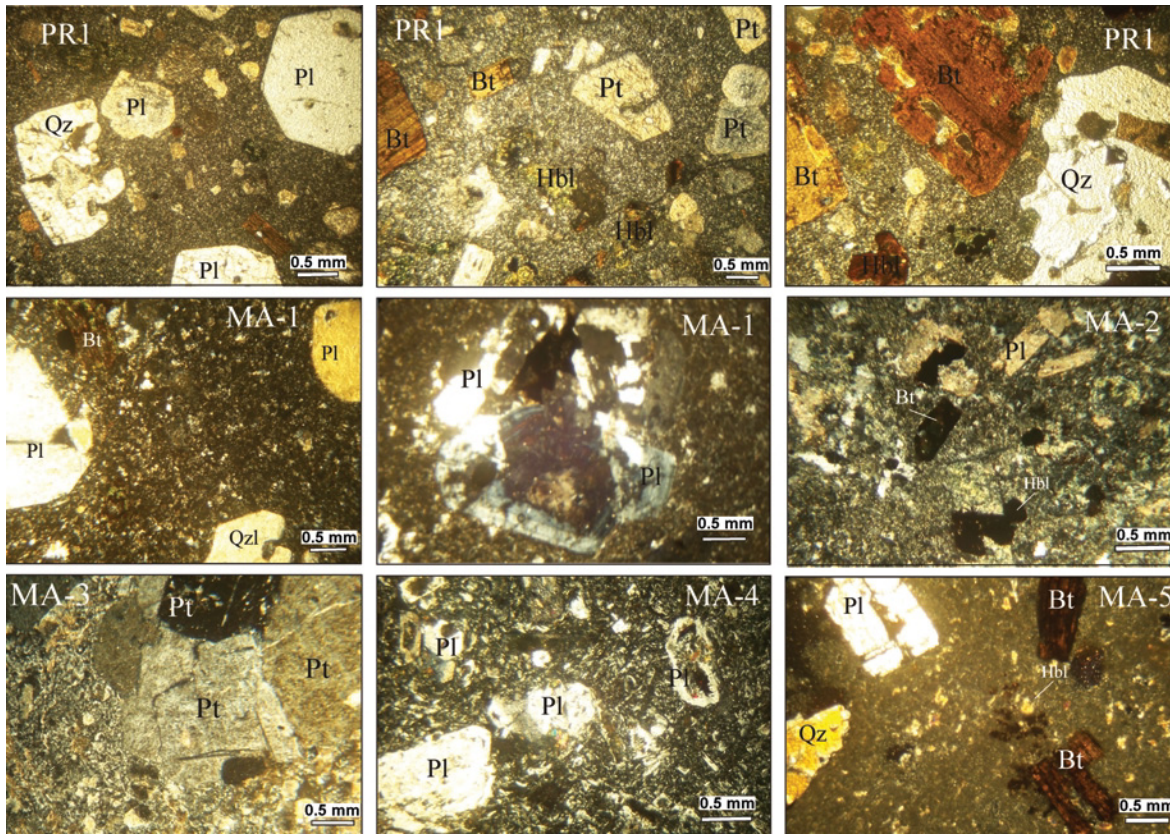

Figure 3. Photomicrographs (crossed nicols) of typical dacite (PR and MA-1–MA-4) and rhyodacite (MA-5) with quartz (Qz), plagioclase (Pl), biotite (Bt), and hornblend (Hbl) phenocryts (abbreviations taken from Whitney and Evans, 2010).

with minor amounts of kaolinite, pyrite, biotite fragments, and silica polymorphs. Purple, white, and pale-green bentonites are interfingered with each other. The Ca-bentonite contains rare kaolinite, albite and silica polymorphs (quartz and opal-CT), with the latter being the most abundant. The Na-bentonite deposits observed in the Kumru district are more homogenous than the Ca-bentonite deposits and contain illite, kaolinite, and albite (Figure 4). The presence of thin coal layers, limestone beds, silicified tree trunks, and silicified layers reveals that Na-bentonite formed in a coastal marsh or shallow-sea environment by hydration of pyroclastic materials during diagenesis and increase in and migration of silica from volcanic ash above and below. The basal spacing (001) of the untreated Ca-montmorillonite varies between 14.97 and 15.12 Å, whereas that of Na-montmorillonite ranges between 13.05 and 12.37 Å (Figure 4). Second-, third-, fourth-, and fifth-order basal reflections can be identified in the XRD patterns of the untreated and ethylene-glycol solvated (EG) samples. In the heated samples, only the first-, second-, and third-order reflections are present (Figure 4). Asymmetries of the basal reflections to the low-angle side of the Na-smectites may be explained by the presence of minor Ca in the interlayers of the smectites, and the d_{060} value of 1.49–1.50 Å indicates a dioctahedral smectite (Wilson, 1987).

The glycolation of the Ca-bentonite caused a shift of the smectite peak from 14.97 to 18.00 Å, and the Na-bentonite caused a shift of the smectite peak from 12.30–12.80 to 17.67 Å (Figure 5). The broadening of all the studied smectite peaks and the high background at low angles may be related to small coherent scattering domains of individual smectite crystals and/or inter-stratification between the smectite and another clay mineral (Moore and Reynolds, 1997). The absence of mixed-layer illite-smectite minerals in the Ca-smectites was inferred from the width of the 001 basal reflection (oriented and ethylene glycol-solvated) and the existence of a rational *d* spacing of the remaining basal reflections. Heating at 490°C resulted in collapsed smectite peaks at 9.73 and 9.89 Å (Figure 5a). The main silica polymorph present in the bentonites is moderately disordered opal-CT, which was identified by the diffuse band centered at ~4.04 Å (with a shoulder near 4.30 Å) and a weaker peak at 2.50 Å in the XRD patterns (Figure 4).

Observations by SEM of the bentonite samples revealed useful information about the micro-texture and alteration processes. The Ca-smectite occurs as thin, popcorn-shaped crystals in a dense aggregate that

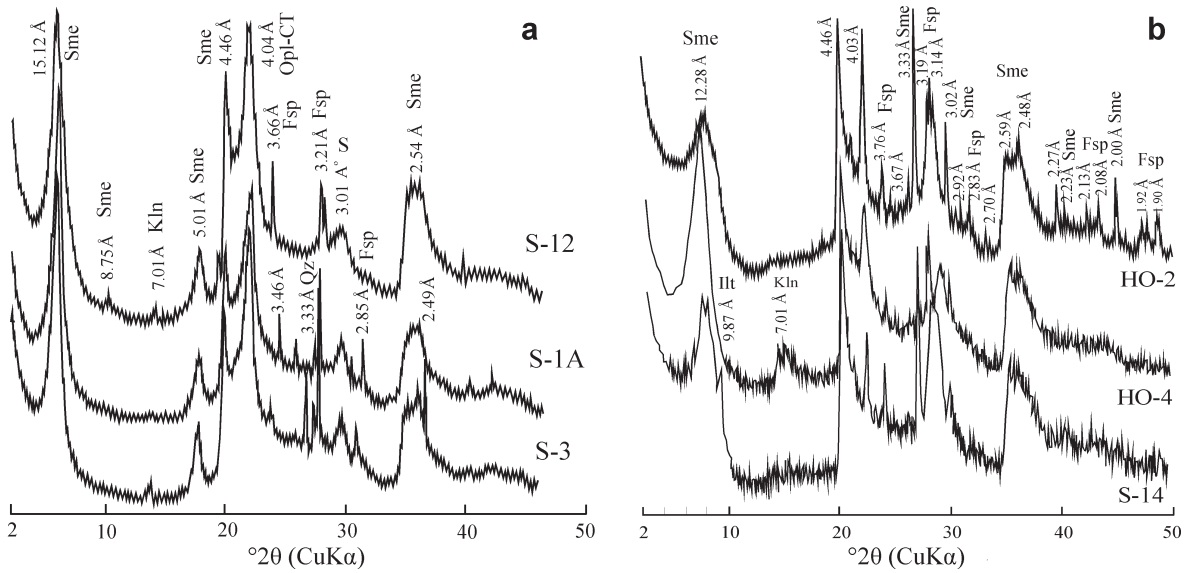

Figure 4. Representative XRD patterns of randomly oriented powders of some pure and nearly pure bulk-rock samples from the study area: (a) Ca-bentonite; (b) Na-bentonite. Fsp: feldspar; Ilt: illite; Kln: clinoptilolite; Opl-CT: opal-CT/tridymite; Qz: quartz; Sme: smectite; (abbreviations from Whitney and Evans, 2010)

displays a honeycomb texture with platy smectite particles (Figure 6). The opal-A and opal-CT were altered to fine aggregates of smectite with a coarse, open honeycomb texture (Figure 6). The opal particles consist of spherical amorphous silica particles with a diameter of ~0.5 μm (opal-A; Florke *et al*., 1991) and opal-CT lepispheres (Wise and Kelts, 1972) with a diameter of 0.5−2.0 μm (Figure 6c,d).

According to SEM studies, alteration commonly began perpendicular to the micro-fractures within the volcanic glass (Figure 6a,b) and altered the glass rapidly to form spongy pseudomorphic textures of smectite and opal-CT (Figure 6c,d). Dissolution and partial conversion of the feldspar were also observed. The alteration textures are common in the Ca-bentonites at Göbü, İncirli, and Ünye localities. Smectite from the Na-bentonite (Kumru bentonite deposits) formed in ultrafine, thin, and rod-shaped habits that display a honeycomb texture (Figure 7). Partial conversion from volcanic glass and euhedral feldspar to montmorillonite was observed (Figure 7a,d). Voids left from the dissolution of hyaloclasts were filled pervasively by fine, honeycomb-textured montmorillonite.

The Ca-bentonite contains a small amount of Fe, Al, Ti, some Mg, and a large amount of Si; the Na-bentonite has the opposite chemical characteristic (Tables 1, 4). The charge deficiency in the octahedral sheet was balanced partially by structural Fe(III) and partially by

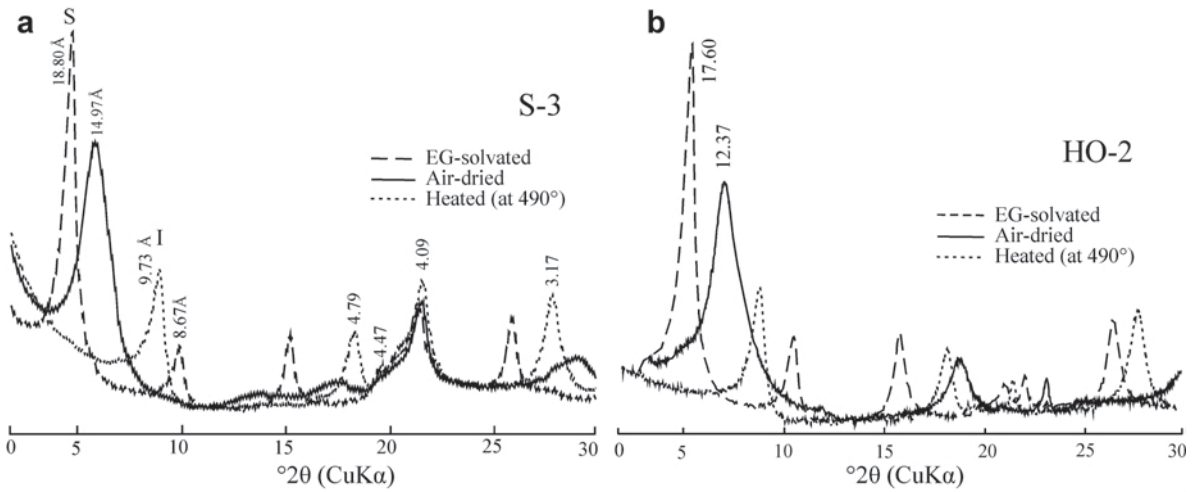

Figure 5. Representative XRD patterns of oriented powder bulk samples of Ca-bentonite (a) and Na-bentonite (b).

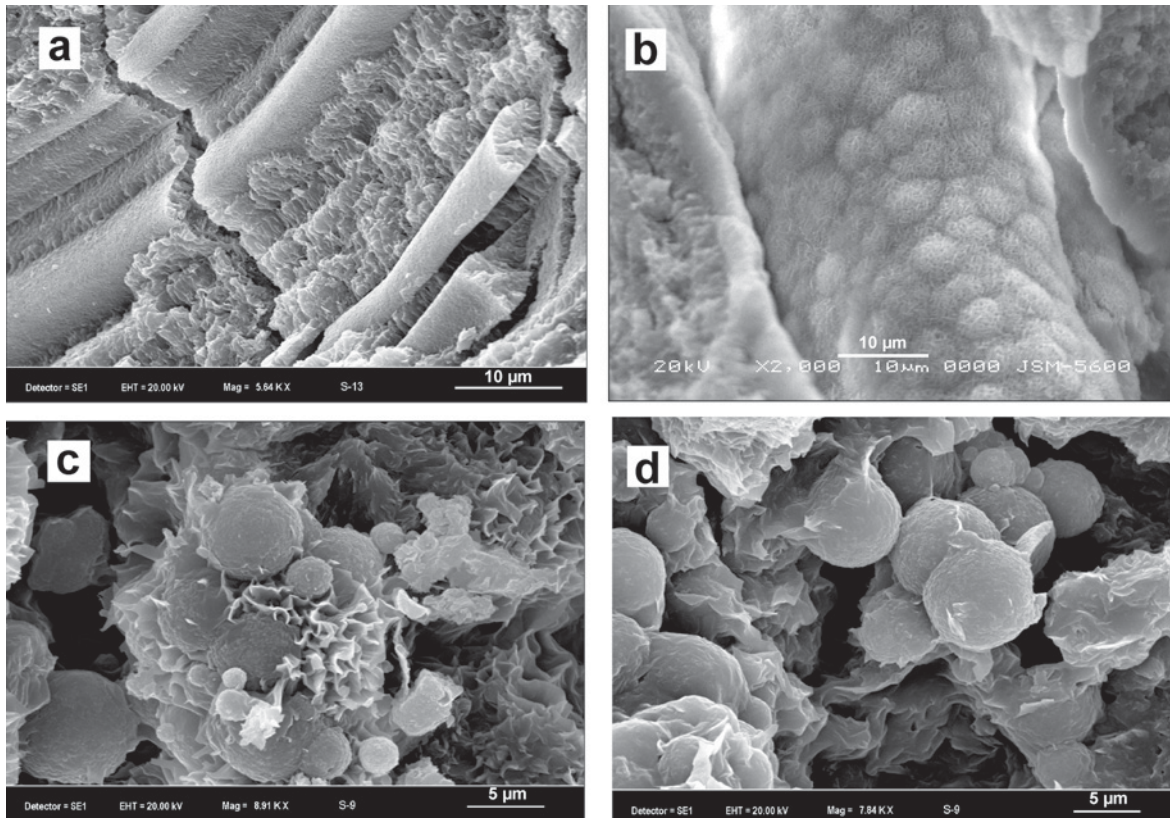

Figure 6. Honeycomb texture with platy smectite particles showing edge-to-edge and edge-to-face contacts. Alteration commonly begins perpendicular to micro-fractures within or on the outer surfaces of the volcanic glass. Pseudomorphic textures resulting from complete replacement of volcanic glass by smectite were partially preserved. The glass shards have been completely altered (a,c) and opal/opal-CT has been altered to montmorillonite. The spherical, botryoidal particles of X-ray amorphous silica with a diameter of ~0.5−5 µm and most of the opal-A and opal-CT lepispheres were tightly packed. (d) Dissolution and transformation of Na-feldspar to montmorillonite.

interlayer cations, mainly by Ca^{2+} but also Na^+ and K^+ in the Ca-smectite and by Na^+ in the Na-montmorillonites.

The structural formulae of the bentonites were calculated on the basis of $O_{10}(OH)_2$ (Weaver and Pollard, 1973) using the chemical composition of the montmorillonites (<2 µm) (Table 4). The remaining portions of the structural formulae for the Na- and Ca-montmorillonites were, therefore,

$$Na_{0.42}Ca_{0.15}K_{0.09}(Si_{3.76}Al_{0.24})(Al_{1.33}Mg_{0.36}Fe_{0.22}Ti_{0.02})$$

and

$$Ca_{0.26}Na_{0.14}K_{0.06}(Si_{3.99}Al_{0.01})(Al_{1.49}Mg_{0.26}Fe_{0.19}Ti_{0.01})$$

respectively.

The substitution of Al for Si in the tetrahedral sheets of Ca-smectite was limited (0.00−0.01) but the octahedral cation composition was generally similar for the two montmorillonites. The Na-montmorillonites are richer in Al_2O_3 than their Ca-counterparts and contain 0.06−0.13 K atoms per formula unit. The smectites contain different tetrahedral charge/octahedral charge ratios. The mean charge ratio is 0.41 in the Na- and 0.02 in the Ca-montmorillonite. The Na-bentonite shows a more pronounced beidellitic character than the Ca-bentonite, which is almost pure montmorillonite (Güven, 1988). The total layer charge of the Na-montmorillonites (mean = 0.82) is greater than that of the Ca-montmorillonites (mean = 0.53) (Table 4).

Geochemistry

Because of the mobility of the major elements during the alteration of the parent rocks, immobile elements were used for chemical and tectonic discriminations. In spite of the differences in major-element concentrations, all of the slightly and moderately altered parent rocks (PR1, PR2, and MPR, respectively) and their alteration products (bentonites) are plotted in the Nb/Y *vs.* Zr/TiO_2 diagram of Winchester and Floyd (1977) (Figure 8). The Ca-bentonites and PR2 are plotted in the trachyte area while PR1, MPR, and Na-bentonites are located in the rhyolite/dacite, andesite and trachyandesite areas. Most of the Na-bentonite samples plotted with the PR1 and MPR while the PR2 and Ca-bentonites plot in different areas from each other. Therefore, the Ca-bentonite

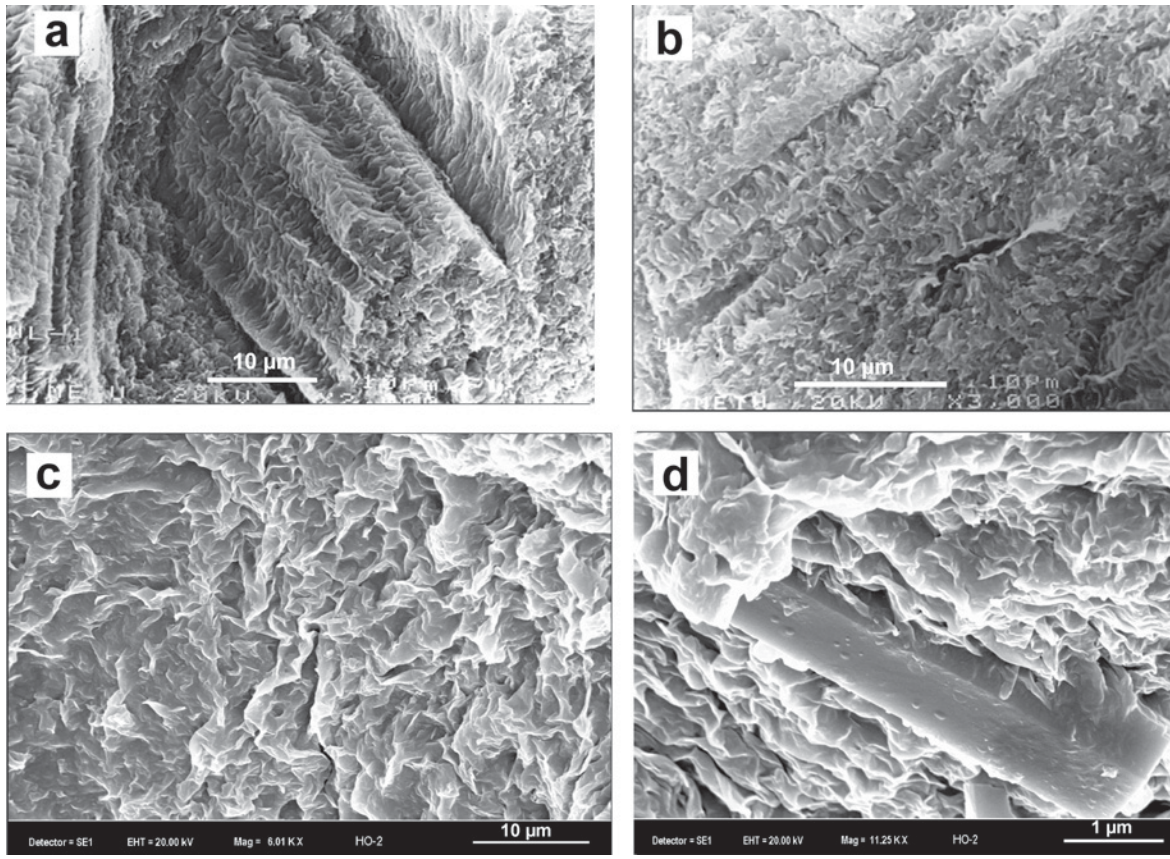

Figure 7. Na-montmorillonite occurs as ultrafine, thin, rod-shaped crystals forming a dense aggregate, with rods in parallel orientation. The inner sides of the rods display a thin, 'popcorn'-shaped habit. Partial conversion of volcanic glass is seen in (d). Silica shards or other rock fragments were rarely observed.

samples derived from a different source rock from the Na-bentonite (Figure 8). All major and trace elements were gained or lost to some extent, so they are mobile in the samples (Table 3). This mobility was attributed to a more alkaline character of back-arc basin during bentonite formation (*e.g.* Christidis, 1998). The ratios

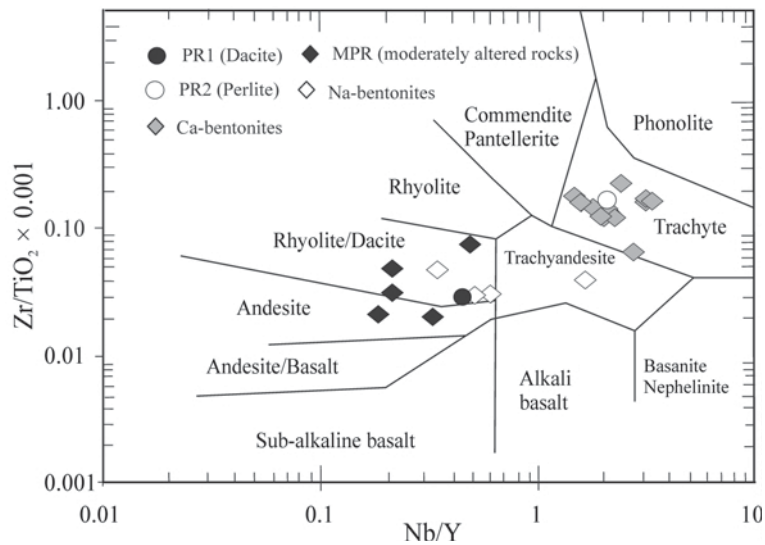

Figure 8. Position of the parent rock, moderately altered rocks, and Na- and Ca-bentonite samples in the diagram of Winchester and Floyd (1977).

Table 4. Chemical analyses (wt.%) and structural formulae of Na- and Ca-montmorillonites.

Samples	Na-bentonites				Ca-bentonites			
Elements	HO-1	HO-2	HO-4	S-14	S-3	S-8	S-9A	S-10
SiO_2	55.20	54.91	54.83	54.98	57.31	58.01	59.02	58.55
Al_2O_3	19.63	19.45	18.79	19.83	18.52	17.93	18.78	18.94
Fe_2O_3	4.29	4.31	4.19	3.86	3.62	2.976	2.78	3.71
MgO	3.75	3.22	3.63	3.69	2.97	2.57	2.36	2.21
CaO	1.33	2.32	2.68	1.87	2.92	3.01	2.87	3.07
Na_2O	3.01	3.78	2.97	2.98	0.44	1.28	1.51	0.82
K_2O	1.48	0.65	1.06	1.18	0.41	1.06	1.01	0.26
TiO_2	0.48	0.43	0.31	0.19	0.10	0.20	0.06	0.20
LOI	6.02	10.7	11.83	11.16	13.70	12.96	11.60	12.91
Total	99.98	99.94	99.97	99.96	99.97	99.98	99.98	99.97
Tetrahedral cations								
Si	3.75	3.75	3.78	3.76	3.96	4.00	4.00	3.99
Al	0.25	0.25	0.22	0.24	0.04	0.00	0.00	0.01
TTC	0.25	0.25	0.22	0.24	0.04	0.00	0.00	0.01
Octahedral cations								
Al	1.32	1.32	1.31	1.35	1.47	1.46	1.49	1.53
Fe	0.22	0.22	0.22	0.20	0.19	0.15	0.24	0.16
Mg	0.38	0.33	0.37	0.38	0.31	0.26	0.25	0.23
Ti	0.02	0.02	0.02	0.01	0.01	0.01	0.001	0.02
TOC	0.52	0.62	0.59	0.55	0.39	0.60	0.61	0.46
Interlayer cations								
Ca	0.10	0.17	0.20	0.14	0.21	0.44	0.21	0.16
Na	0.40	0.50	0.40	0.39	0.06	0.17	0.20	0.12
K	0.13	0.06	0.06	0.10	0.04	0.09	0.09	0.03
ILC	0.72	0.90	0.85	0.73	0.52	0.71	0.70	0.47
TLC	0.77	0.89	0.81	0.79	0.43	0.60	0.61	0.47
Ca/Na	0.25	0.34	0.50	0.36	3.50	2.56	1.05	1.33

TTC: total tetrahedral sheet charge; TOC: total octahedral sheet charge; ILC: interlayer charge; TLC: total layer charge.

of Zr/TiO_2 in PR and MPR are almost constant, whereas the Nb/Y ratio varies (Figure 8). Plots of PR in different areas in the diagrams may be related to different behaviors of Zr, Nb, Ti, and Y during alteration.

Mass-balance calculations show that all major-element oxides changed in nearly all of the sample groups. Progressive alteration of PR2 caused depletion in alkaline oxides (K_2O and Na_2O) and enrichment in alkaline earth oxides (CaO and MgO) in all of the Ca-bentonite samples derived from PR2. Na_2O was depleted in all of the Na-bentonites and in most of the MPR. In the Na-bentonites, the *MREE* and *HREE* contents changed whereas *HREE* were virtually immobile in the Ca-bentonites. The *REE* and TRE contents mostly increased in the Ca-bentonites in contrast to the Na-bentonites. The HFSE were virtually immobile while LILE were strongly depleted in all of the bentonites. The *LREE*, *MREE*, and *HREE* were strongly depleted in most of the MPR samples (Figure 2).

TiO_2, MnO, Lu, Tm, and Tb were immobile in all samples. The enrichment of Nb, Ta, and Hf in Ca-bentonite was much greater than in the Na-bentonite, and these elements were completely depleted in MPR samples. Zr content increased, especially in the Ca-bentonite (Table 3). According to mass balance calculations, Al_2O_3, Zr, Nb, Hf, Y, Yb, L*REE*, and *MREE*, which previously were thought to be immobile during hydrothermal alteration processes (*e.g.* Rollinson, 1993; Floyd and Winchester, 1978; Corfu and Davis, 1991), apparently were mobile here. This mobility phenomenon has been reported previously by several authors (e.g. Hynes, 1980; Murphy and Hynes, 1986; Jiang, 2000; Jiang *et al*., 2003, 2005; Salvi *et al*., 2000; Salvi and Williams-Jones, 1996; Patino *et al.*, 2003; Torres-Alvarado *et al.*, 2007). Fe_2O_3 and P_2O_5 were moderately positively correlated with *REE* (Fe = 0.56; P = 0.47) and *LREE* (Fe = 0.59; P = 0.49) in the Ca-bentonites, suggesting that the *LREE* distribution was related to Fe-, Ti-, and P-bearing minerals, whereas in the Na-bentonites, the *REE* show moderately positive correlation with only MnO. The LILE show strongly positive correlation with only Na_2O in the Ca-bentonites, and weakly negative correlation in the Na-bentonite (Table 2).

The *REE*, LILE, and HFSE were normalized to chondrite (Boynton, 1984; Sun and McDonough, 1989).

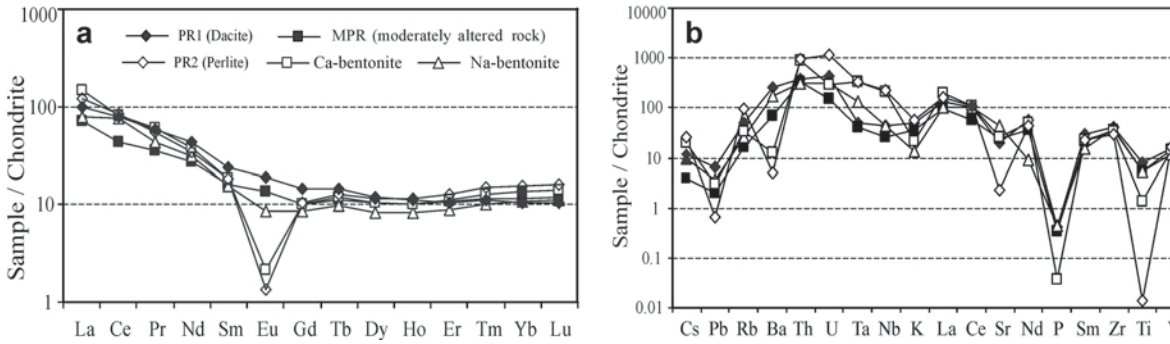

Figure 9. (a) Chondrite-normalized *REE* pattern of the investigated sample groups (normalization values from Boynton, 1984). (b) Chondrite-normalized trace elements and *REE* diagram of sample groups (normalization values from Sun and McDonough, 1989). The data were taken from Table 1.

The normalization of all sample groups showed very similar trace-element and *REE* patterns. All *REE* were enriched compared to chondrite, and the enrichment ratios of the *LREE* were greater than those of the *HREE*, which displayed virtually flat patterns (Figure 9a). The HFSE, other than P, in all of the samples are enriched relative to chondrite (Figure 9b). The depletion of HFSE with respect to LILE and *REE* yielded small values for $(Nb/Ba)_{cn}$ (0.17, 0.3, and 0.25) for all samples except Ca-bentonite, which has a ratio of 16.0. This phenomenon was also supported by the ratios of $(Nb/La)_{cn}$ = 0.35, 0.27, 0.42, and 1.08; $(Sr/La)_{cn}$ = 0.16, 0.26, 0.41, and 0.13; and $(Ti/Sm)_{cn}$ = 0.26, 0.26, 0.35, and 0.06.

REE fractionation is less in the MPR and Na-bentonites than those of the Ca-bentonites and this trend may be related to the lesser *REE* fractionation of the PR1 with $(La/Yb)_{cn}$ = 3.50 than in the PR2 with $(La/Yb)_{cn}$ = 7.75. The $(La/Yb)_{cn}$ ratios of the samples indicated that the *LREE* were enriched particularly strongly in the Ca-bentonite (10.99) and weakly in MPR (6.41). The $(La/Sm)_{cn}$ ratio showed fractionation of the *LREE* to *MREE* in the Na-bentonite and Ca-bentonite in accordance with *LREE* fractionations of PR1 and PR2. The $(Gd/Yb)_{cn}$ ratio of the Ca-bentonite and PR2 indicated that the *HREE* were less enriched than *LREE* in all of the bentonites (Table 1). The *HREE* fractionation of the samples was generally small (Table 1). The ratios of $(La/Sm)_{cn}$, $(La/Yb)_{cn}$, $(Gd/Yb)_{cn}$, and $(La/Lu)_{cn}$ in PR1, PR2, MPR, Na-bentonite, and Ca-bentonite indicated *LREE* enrichment over *MREE* and *HREE* and a slight enrichment of *MREE* relative to *HREE* (Table 1, Figure 10) (Christidis, 1998).

Another significant feature of the dacitic parent rock, the MPR, and the Na-bentonites is the depletion of LILE with respect to *LREE*, resulting in relatively small Rb/La, Ba/La, K/La, and Th/La ratios relative to PR1. In the perlite parent rock and the Ca-bentonites, the depletion of LILE with respect to *LREE* resulted in relatively small Rb/La, K/La, and Th/La ratios relative to PR2, except Ba/La is greater than in the PR2. The Th/La ratio is large in the MPR and Na-bentonites, except for two samples of the MPR, but is small in the Ca-bentonites (Table 1). The total *REE* concentration of Ca-bentonite is greater than in the Na-bentonite.

The PR1 is characterized by a *LREE*-enriched pattern with a slightly positive Eu* anomaly. The Eu anomaly was calculated by the formula $Eu/Eu^* = Eu_N/(Sm_N \times Gd_N)^{1/2}$. The MPR and Na-bentonite have slightly negative Eu* anomalies (Eu/Eu* <1) while the PR2 and the Ca-bentonite have strongly negative Eu*

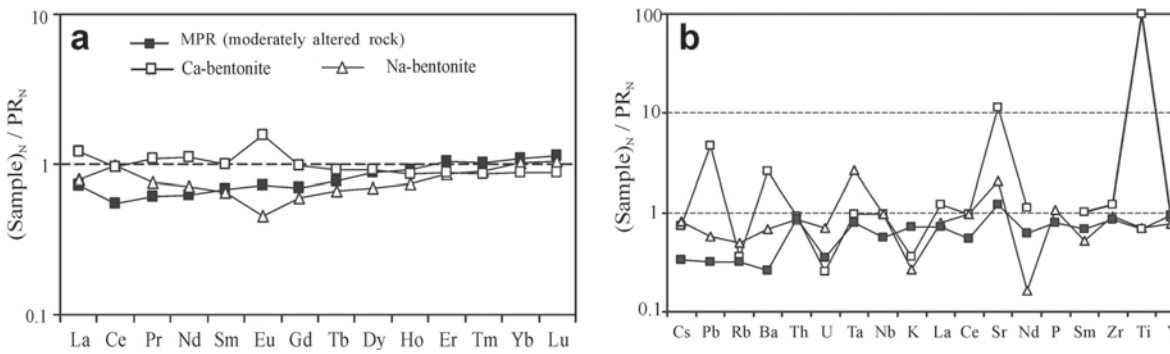

Figure 10. (a) Parent-rock-normalized *REE* patterns of the investigated sample groups. (b) Parent-rock-normalized trace elements diagram of sample groups. The data were taken from Table 1.

anomalies. The Ce anomaly denoted Ce/Ce* was calculated by $Ce/Ce^* = Ce_N/(La_N \times Pr_N)^{1/2}$.

No Ce anomalies were observed in any of the MPR samples except for MA-5 (0.68). The Na-bentonite showed a weakly positive Ce anomaly (Ce/Ce* = 1.27), and the PR2 (1.04) and most of the Ca-bentonite displayed moderately negative Ce anomalies ranging from 0.60 to 1.21 (Table 1).

Depletion of LILE over *LREE* in PR1, PR2, MPR, Na-bentonite, and Ca-bentonite resulted in $(K/La)_{cn}$ = 0.39, 0.37, 0.38, 0.13, and 0.11; in $(Rb/La)_{cn}$ = 0.40, 0.60, 0.17, 0.24, and 0.18; in $(K/La)_{cn}$ = 0.39, 0.38, 0.13, and 0.11; and in $(Rb/La)_{cn}$ = 0.4, 0.17, 0.24, and 0.18.

With the exception of several properties, the parent-rock-normalized *REE* patterns of all the samples were similar to each other and are characterized by virtually flat patterns, especially in *HREE*. The Eu anomalies are significantly more apparent in the Ca-bentonite (1.59) and Na-bentonite (0.72) than in the MPR (1.06) (Figure 10a). The parent-rock-normalized trace element patterns of the MPR and Na-bentonites are similar while the pattern of the Ca-bentonite is clearly different from those of the others. The Cs, Rb, U, and K were depleted slightly in all samples. Ti, Pb, and Ba were enriched in the Ca-bentonite. Zr and Y were also unchanged, but this does not necessarily mean immobile. This behavior may be a result of removal of some major elements (*e.g.* Al_2O_3, MgO, CaO, Na_2O, K_2O) from the parent rocks and subsequent decrease of the rock volume during the alteration. In such a case, even though a less mobile element has been depleted, it may be seen as immobile in the new, decreased rock volume.

DISCUSSION

The presence of unaltered perlitic materials in the Ca-bentonite and disseminated Ca-bentonite in the perlite indicate that the alteration occurs mainly as an effect of gases and vapors in the parent rocks before cooling (Grim and Güven, 1978). In addition, hydrothermal fluids and marine-water activities may have played an important role in the alteration of the perlitic rocks to the Ca-bentonite. Mineral formation depends on the composition of the gases and vapors and/or on the changing of migration and local remobilization of alkaline and alkaline earth elements. The Ca-bentonite deposits contain vertical fractures >30 cm wide. These fractures are sometimes filled with aragonite/calcite. Stocks 5−10 m in diameter occur sporadically in association with these fractures. The stocks indicate that hot springs circulated upward through the parent rock. Ca-bentonite formation was also related to the outlet of bicarbonate water through fractures in the contact zone between the pyroclastic materials and the lavas. The geologic findings agree with the suggested explanation by Caballero *et al.* (2005). The Ca-bentonite probably resulted from both the deuteric action and hydrothermal activity when alkalis had been leached and Ca and Mg were enriched significantly during alteration of perlite to Ca-bentonite. The major elements Al and Fe were enriched in the Ca-bentonites, and Al and Fe show different behaviors in the Na-bentonite. Ca and Mg were enriched in all of the Ca- and most of the Na-bentonites while alkalis were leached. Si shows different behaviors in the Na- and Ca-bentonites. Christidis *et al.* (1995) reported that during bentonite formation (with or without zeolites) from rhyolitic parent rocks, the alkalis and Si migrated; Mg, Fe, and Ca were enriched; and Al and Ti were also immobile. Gains and losses of elements are attributed to alteration processes under open-system conditions (Münch *et al.*, 1996). Magnesium, Ca, and Fe were enriched and probably fixed by structural incorporation during bentonite formation, in agreement with suggestions by Zielinski (1982) and Christidis (1998).

Zirconium has been regarded as an immobile element (Pearce and Cann, 1973), but Finlow-Bates and Stumpfl (1981) suggested that Zr and Ti can be mobile during hydrothermal alteration, depending on the pH. Rubin *et al.* (1993) explained that Zr can be mobile in hydrothermal systems that develop in a broad range of igneous geochemical environments. The Zr/Hf ratios of MPR (mean = 36.1) and Na-bentonite (mean = 34.3) are similar to that for PR1 (mean = 35.4), and the ratio of the Ca-bentonite, which ranges from 21.2 to 31.0 (mean = 26.9), is similar to that for PR2 (mean = 24.71). The Zr/Hf ratios of the PR1, MPR, and Na-bentonite samples are similar to those of andesitic rocks (~40; Gill, 1981). The ratios of the PR2 and the Ca-bentonite are smaller than that of the andesitic rock. The different Zr/Hf ratios of the Na- and the Ca-bentonites may be related to different parent rocks and also to the various alteration processes of the volcanic rocks.

The similarity of *REE* patterns resulting from alteration by alkaline or acid fluids suggests that the shape of *REE* trends was controlled principally by fluid/rock ratios and secondly by mineralogy (Hopf, 1993). The relevant *HREE* fractionation with respect to the *LREE* in the advanced argillic facies is mainly because of the presence of secondary P and Fe minerals, which can fix the *LREE* into their structures, in the present case, montmorillonite. If mass-balance calculations are taken into consideration, although *REE* were enriched during alteration, the chondrite-normalized *REE* patterns of the MPR and Na-bentonites show close similarity to that of PR1 and the chondrite-normalized *REE* patterns of Ca-bentonites are similar to that of PR2. The chondrite-normalized *REE* patterns provide evidence of *REE* enrichment in all the sample groups; in particular the *LREE* and some of the *MREE* were enriched relative to *HREE*. This tendency may be related to the almost uniform alteration mineralogy which resulted from pervasive alteration of the parent rocks (Figure 9a). These trends may be inherited from the *REE* characteristics of the parent rocks. In addition, under alkaline conditions, the stability of the *HREE* complexes in

solutions is greater than that of the *LREE* complexes (Ronov *et al.*, 1967). The vertical shift in *LREE* and sub-parallel trends to PR1 and PR2 are present in nearly all of the sample groups (except for the Eu anomaly in the Ca-bentonite) and may be due, in part, to the similar primary composition of the different source rocks. These *REE* trends of the altered rocks may also have been inherited from the parent-rock *REE* signatures. The characteristic features of *REE* patterns (*LREE* enrichment relative to *HREE* and flat *HREE*) may be attributed to the felsic origin of the parent rocks. The similarity of the chondrite- and parent-rock-normalized trace and *REE* patterns of all sample suites indicates similar source rocks such as dacite and perlite. The relative flatness of the patterns in the PR-normalized plots indicates that the *HREE*, *MREE*, and some of the *LREE* were relatively unchanged, especially in Ca-bentonite, during alteration and bentonite formation. The difference among the parent-rock- and chondrite-normalized trace and *REE* patterns, and mass-balance calculation histograms can be explained by a huge amount of remobilization of some major elements from the parent rocks (*e.g.* Al_2O_3, MgO, CaO, Na_2O, K_2O) and further decrease in the total volume of the parent rock during alteration (Figures 9, 10). The mass calculation gives the most reliable results for element mobility because of the use of immobile element pairs.

Silica enrichment in most of the bentonite samples relative to the parent rock may be related to the fact that silica has not been removed from the system and subsequent transportation through geothermal waters as shown by the presence of silicified tree trunks and silicified layers in the Na-bentonites. During the initial stage of alteration volcanic vapors and hydrothermal solutions were abundant in the system and were probably acidic. Therefore, alkaline elements, but only insignificant amounts of silica, were leached from the parent rocks. Thus, the pH of the solution gradually became alkaline with dissolution of the alkalis, and montmorillonites may have been precipitated simultaneously from solution. The vertical uniformity of the mineral composition of the bentonites suggests pervasive alteration of the parent rocks. The perlite relicts in the Ca-bentonite indicate that the formation of Ca-bentonite may be related to alteration of the perlite. The alteration was dominated by the reaction of gases, vapors, and hydrothermal solutions within the parent rock and its pyroclastic counterparts (Grim and Güven, 1978).

The layer charge of Ca-montmorillonite is smaller than the average charge of the Na-montmorillonite (0.60) in Na-bentonites. The tetrahedral occupancy of Si in Ca-smectite is high because of the X-ray amorphous and partially amorphous silica content (opal-A, opal-CT) of the Ca-bentonites. Some of the amorphous silica, the particle size of which was <2 μm, was not removed from the clay fraction during preparation of clay-size phase. The Ca/Na ratios of montmorillonites are different in the different smectites. The ratios range from 0.25 to 0.50 in Na-montmorillonites, and they vary from 1.05 to 3.50 in Ca-montmorillonites. Shirozu and Iwasaki (1980) and Inoue *et al.* (1984, 1987) demonstrated that the Ca/Na ratio of smectite in Kuroko-type hydrothermal alteration decreased systematically from the inner to the outer portion of the marginal smectite zone. The greater Mg concentrations in the Na-bentonite relative to the Ca-bentonite may be attributed to the circulation of groundwater, especially groundwater of marine origin. In addition, some of the Mg may have been supplied from sea water or hydrothermal solutions in different domains of the altered rocks. Mg^{2+} was moved rapidly from sea water into secondary minerals such as smectite or chlorite. The layer charge of the montmorillonites, which was calculated from the chemical analysis of the clay-size fraction, was >0.46 (Table 4). The layer charges of the montmorillonites indicate that the montmorillonite is mainly of hydrothermal origin (Weaver, 1989; Inoue, 1995). The Fe(III) contents in the octahedral sheet of the Na- and Ca-montmorillonites range from 0.20 to 0.22 and from 0.15 to 0.24, respectively. The Si content of the tetrahedral sheet of the Na-and Ca-montmorillonites varies from 3.75 to 3.78 and 3.96 to 4.00, respectively, suggesting that they were derived from intermediate to acidic source rocks (Christidis and Huff, 2009).

According to the mass-balance calculations, the strong depletion of the *REE* resulted mainly from decreasing *LREE* and partially from decreasing *MREE* in all of the MPR samples. The moderate enrichment in Ca-bentonites and slightly in Na-bentonites suggests that the *REE* were mobilized in the system at the beginning of the alteration. These *REE* may have been either partially fixed or adsorbed by clay minerals or may be hosted in accessory minerals such as monazite, which are not affected significantly by alteration. The greater content of *LREE*, *MREE*, *HREE*, and HFSE of Ca-bentonites relative to Na-bentonites may be related to alteration intensity. PR1 and PR2 were the original parent rocks, and they have different Eu anomalies. PR1 has a slightly positive anomaly, and PR2 has a strongly negative Eu anomaly. The depletion in Eu may have resulted from dissolution of a Eu-rich mineral (*e.g.* feldspar) by hydrothermal fluids (Lewis *et al*., 1997). Hydrothermal fluids preferentially leach Eu relative to other *REE* (Svarjensky, 1984; Bau, 1991). The negative Eu anomalies become more apparent with depletion of Na_2O and CaO, suggesting that these element oxides were released at least partially in response to destruction of plagioclase, which hosts most of the Eu. This result also suggests felsic source rocks (Tables 1, 3, Figure 9a). The slightly positive Eu* anomaly of the PR1 may be related to the weak alteration of plagioclase in the PR1 by hydrothermal fluids. In Ca-bentonite, Sr^{2+} shows a moderately positive correlation (r = 0.51) with the Eu* anomaly, and in Na-bentonite, this correlation is strongly

positive (r = 0.98). The anomaly of Eu/Eu* varies from 0.09 to 0.26 in Ca-bentonite and it ranges from 0.77 to 1.04 in Na-bentonite. The strongly negative Eu anomaly of the Ca-bentonite may be inherited from the PR2 with a strong Eu anomaly which resulted from the reducing environmental conditions during the formation of perlite (Table 1). Eu^{3+} was, therefore, converted to Eu^{2+} and retained in the post-magmatic hydrothermal solution. Some of the leached Ca^{2+} was located in the exchange sites of smectite, and a large amount of the Ca^{2+} may have been precipitated as aragonite/calcite in some fractures. This type of precipitation may have been supported by a hydrothermal solution that was circulating deeply and carrying elements, such as Ca and Na.

The PR1, PR2, four samples of MPR, and all of the Na-bentonite samples have a positive Ce anomaly. Most of the Ca-bentonite samples show slightly negative Ce anomalies (0.9), which may be an artifact of analytical precision (the detection limit of Ce is 0.02 ppm, Table 1). The positive Ce anomalies of the Na-bentonites may be related to reducing environmental conditions such that the Ce^{3+} was not converted to Ce^{4+} during the alteration (Braun *et al.*, 1990; Class and la Roex, 2008).

CONCLUSIONS

Although the HFSE, LILE, TRE, and *REE* concentrations of the sample suites were highly variable, their chondrite-normalized trace and *REE* patterns were similar. Strong or moderate enrichment, except Eu in PR2 and Ca-bentonite, was observed in the chondrite-normalized *REE* patterns of all the sample suites. This result suggests that significant mobilization or fractionation of the *REE* took place during alteration. The similarity of the trends for *REE* and for Ti, P, Nb, Sr, Th, U, Rb, Cs, Pb, and Y in all of the bentonite samples indicates that the sampled bentonites were derived from different parent rocks such as dacite and perlite, but the alteration occurred under different conditions and/or environments.

The Ca-bentonite was formed by *in situ* alteration from perlite in the volcanic belt, and the Na-bentonite was formed by hydration and diagenesis in fore-arc fill deposits intercalated with mudstone, marl, and limestone. The formation of the Ca-bentonitic clays in the Eastern Pontides is related to the hydrothermal processes. The Ca-bentonite is not mono-mineralic but gradually passed through to parent rocks, indicating that they were formed mainly by hydrothermal alteration. The Na-bentonite is generally more pure than the Ca-bentonite and is closely related to the non-volcanic sediments in the back arc basin (*i.e.* marl and limestone). The results of the mass-balance calculation for *REE*, TRE, and HFSE of the bentonite support the suggestion that the Ca-bentonite originated from *in situ* alteration of perlite. The Cu, Pb, Zn, and Ni are depleted in the Na-bentonites and enriched in the Ca-bentonites. The greater mineralogical homogeneity of the Na-bentonite than that of the Ca-bentonite throughout the deposits suggests that the volcanic material was altered in stable chemical conditions imposed by the sedimentary environment.

ACKNOWLEDGMENTS

The present investigation was made possible by the partial financial support of TUBITAK (The Scientific and Technical Research Council of Turkey; project numbers YDABÇAG-139 and 103Y016). This work was also partially supported by Selçuk University Scientific Research projects support program (09101043 and 09101044). The authors are indebted to two anonymous reviewers for their comments and to the Editors for their careful editorial input and constructive suggestions which improved the quality of the manuscript.

REFERENCES

Arslan, M. and Abdioğlu, E. (2005) Mineralogy, geochemistry and genesis of bentonites of the Ordu area, NE Turkey. *Clay Minerals*, **40**, 131–151.

Bau, M. (1991) Rare-earth element mobility during hydrothermal and metamorphic fluid–rock interaction and the significance of the oxidation state of europium. *Chemical Geology*, **93**, 219–230.

Boynton, W.V. (1984) Geochemistry of rare earth elements: meteorite studies. Pp. 63–114 in: *Rare Earth Element Geochemistry* (P. Henderson, editor). Elsevier, Amsterdam.

Braun, J.-J., Pagel, M., Muller, J.-P., Bilong, P., Michard, A. and Guillet, B. (1990) Cerium anomalies in lateritic profiles. *Geochimica et Cosmochimica Acta*, **54**, 781–795.

Caballero, E., Jimanez de Cisneros, C., Huertas, F.J., Huertas, F., Poszzuoli, A. and Linares, J. (2005) Bentonites from Cabo de Gata, Almeria, Spain: a mineralogical and geochemical overview. *Clay Minerals* **40**, 463–480.

Çağatay, M.N. (1993) Hydrothermal alteration associated with volcanogenic massive sulfide deposits. Examples from Turkey. *Economic Geology*, **88**, 606–612.

Çelik, M., Karakaya, N. and Temel, A. (1999) Clay minerals in hydrothermally altered volcanic rocks, eastern Pontides, Turkey. *Clays and Clay Minerals*, **47**, 708–717.

Chamley, H. (1989) *Clay Sedimentology*. Springer, Berlin, 623 pp.

Christidis, G. E. (1998) Comparative study of the mobility of major and trace elements during alteration of an andesite and a rhyolite to bentonite, in the islands of Milos and Kimolos, Aegean, Greece. *Clays and Clay Minerals*, **46**, 379–399.

Christidis, G.E. and Huff, W.D. (2009) Geological aspects and genesis of bentonites. *Elements*, **5**, 93–98.

Christidis, G. and Warren, D.H. (2009) Geologic aspects and genesis of bentonites. *Elements*, **5/2**, 93–98.

Christidis, G.E., Scott, P.W., and Marcopoulos, T. (1995) Origin of the bentonite deposits of Eastern Milos, Aegean, Greece: geological, mineralogical and geochemical evidence. *Clays and Clay Minerals* **43**, 63–77.

Class, C. and la Roex, A.P. (2008) Ce anomalies in Gough Island lavas – trace element characteristics of a recycled sediment component. *Earth and Planetary Science Letters*, **265**, 475–486.

Corfu, F. and Davis, D.W. (1991) Comment on "Archaean hydrothermal zircon in the Abitibi greenstone belt: constraints on the timing of gold mineralization" by J.C. Claoue-Long, R.W. King and R. Kerrich. *Earth and Planetary Science Letters*, **104**, 545–552.

Ddani, M., Meunier, A., Zahraoui, M., Beaufort, D., El Wartiti, M., Fontaine, C., Boukili, B., and El Mahi, B. (2005) Clay mineralogy and chemical composition of bentonites from the Gourougou volcanic massif (northeast Morocco). *Clays and Clay Minerals*, **53**, 250–267.

Finlow-Bates, T. and Stumpfl, E.F. (1981) The behaviour of so-called immobile elements in hydrothermally altered rocks associated with volcanogenic submarine-exhalative ore deposits. *Mineralium Deposita*, **16**, 319–328.

Florke, O.W., Martin, G.B., Bochum, R., and Wirth, R. (1991) Nomenclature of micro- and non-crystaline silica minerals, based on structure and microstructure. *Neues Jahrbuch für Mineralogie-Abhandlungen*, **163**, 19–42.

Floyd, P.A. and Winchester, J.A. (1978) Identification and discrimination of altered and metamorphosed volcanic rocks using immobile elements. *Chemical Geology*, **21**, 291–306.

Gill, J.B. (1981) *Orogenic Andesite and Plate Tectonics*. Springer, New York, 390 pp.

Gökçe, A. and Bozkaya, G. (2003) Fluid inclusion and stable isotope characteristics of the Inler Yaylası lead-zinc deposits, northern Turkey. *International Geology Review*, **45**, 1044–1054.

Grim, R.E. (1968) *Clay Mineralogy* (2nd edition). McGraw-Hill, New York, 596 pp.

Grim, R. and Güven, N. (1978) *Bentonite: Geology, Mineralogy, Properties and Uses*. Developments in Sedimentology, **24**, Elsevier, New York, 256 pp.

Güven, N. (1988) Smectites. Pp. 497–559 in: *Hydrous Phyllosilicates* (S.W. Bailey, editor). *Reviews in Mineralogy*, **19**. Mineralogical Society of America, Washington, D.C.

Hopf, S. (1993) Behaviour of rare earth elements in geothermal systems of New Zealand, *Journal of Geochemical Exploration*, 47, 333–357.

Hora, Z.D. (1998) Bentonite. *Geological Fieldwork 1997.* pp. 24C1–24C3. British Columbia Ministry of Employment and Investment Paper **1998-1**.

Hynes, A. (1980) Carbonatization and mobility of Ti, Y and Zr in Ascot Formation metabasalts, SE Quebec. *Contributions to Mineralogy and Petrology*, **75**, 79–87.

Inoue, A. (1995) Formation of clay minerals in hydrothermal environments. Pp. 268–303 in: *Origin and Mineralogy of Clays* (B. Velde, editor). Springer, Berlin.

Inoue, A., Utada, M., and Kusakabe, H. (1984) Clay mineral composition and their exchangeable interlayer cation composition from altered rocks around the Kuroko deposits in the Matsumine-Shakanai-Matsuki area of the Hokuroku district. *Japan Journal of Clay Science Society Japan*, **24**, 69–77.

Inoue, A., Kohyama, N., Kitagawa, R., and Watanabe, T. (1987) Chemical and morphological evidence for the conversion of smectite to illite. *Clays and Clay Minerals*, **35**, 111–120.

Jenner, G.A. (1996) Trace element geochemistry of igneous rocks: geochemical nomenclature and analytical geochemistry. Pp. 51–77 in: *Trace Element Geochemistry of Volcanic Rocks: Applications for Massive Sulfide Exploration* (D.A. Wyman, editor). Geological Association of Canada Short Course Notes, **12**.

Jiang, S.-Y. (2000) Controls on the mobility of high field strength elements (HFSE), U, and Th in an ancient submarine hydrothermal system of the Proterozoic Sullivan Pb-Zn-Ag deposit, British Columbia, Canada. *Geochemistry Journal*, **34**, 341–348.

Jiang, N., Sun, S., Chu, X., Mizuta, T. and Ishiyama, D. (2003) Mobilization and enrichment of high-field strength elements during late- and post-magmatic processes in the Shuiquangou syenitic complex, Northern China. *Chemical Geology*, **200**, 117–128.

Jiang, S.Y., Wang, R.C., Xu, X.S., and Zhao, K.D. (2005) Mobility of high field strength elements (HFSE) in magmatic-, metamorphic-, and submarine-hydrothermal systems. *Physics and Chemistry of the Earth*, **30**, 1020–1029.

Karakaya, N. and Karakaya, M.C. (2001a) Hydrothermal alteration of the Şaplıca volcanic rocks, Şebinkarahisar, Turkey. *International Geology Review*, **43**, 953–962.

Karakaya, N. and Karakaya, M.C. (2001b) Mineralogic and geochemical properties of hydrothermal alteration types of Şaplıca (Şebinkarahisar, Giresun) volcanites. *Geological Bulletin of Turkey*, **44**, 75–89.

Karakaya, M.Ç., Karakaya, N., and Ekmekçi, M. (2005) *Doğu Karadeniz Bölgesindeki Bazı Maden Yatakları ile Yüzey ve Yeraltısuyu Kimyası Arasındaki İli*şkinin Araştırılması. TÜBİTAK YDABÇAG-103Y016, Turkey, 159 pp.

Karakaya, N., Karakaya, M.C., Nalbantçılar, M.T., and Yavuz, F. (2007) Relation between spring-water chemistry and hydrothermal alteration in the Şaplıca volcanic rocks, Şebinkarahisar (Giresun, Turkey). *Journal of Geochemical Exploration*, **93**, 35–46.

Keskin, İ., Yergök, F.A., Kara, H., Dönmez, M., and Arslan, M. (1998) Ünye-Fatsa-Kumru-Korgan (Ordu) dolayının jeolojisi. MTA Raport 10182 (unpublished).

Ketin, I. (1966) Tectonic units of Anatolia. *Bulletin of Mineral Research and Exploration*, **66**, 23–34.

Lewis, A.J., Palmer, M.P.R., Sturchio, N.C., and Kemp, A.J. (1997) The rare earth element geochemistry of acid-sulphate and acid-sulphate-chloride geothermal systems from Yellowstone National Park, Wyoming, USA. *Geochimica et Cosmochimica Acta*, **61**, 695–706.

Lombardi, B., Baschini, M., and Torres Sánchez, R.M. (2003) Bentonite deposits of Northern Patagonia. *Applied Clay Science* **22**, 309– 312

MacLean, W.H. (1990) Mass change calculations in altered rock series. *Mineralium Deposita*, **25**, 44–49.

MacLean, W.H. and Kranidiotis, P. (1987) Immobile elements as monitors of mass transfer in hydrothermal alteration. Phelps Dodge massive sulfide deposits, Matagami, Quebec. *Economic Geology*, **82**, 951–962.

Millot, G. (1970) *Geology of Clays*. Springer, Berlin, New York; Masson, Paris, 425 pp.

Moore, D.M. and Reynolds, R.C. (1997) *X-ray Diffraction and the Identification and Analysis of Clay Minerals*, 2nd edition. Oxford University Press, New York, 378 pp.

Murphy, J.B. and Hynes, A. (1986) Contrasting secondary mobility of Ti, P, Zr, Nb and Y in two metabasaltic suites in the Appalachians. *Canadian Journal of Earth Sciences*, **23**, 1138–1144.

Münch, P., Duplay, J., and Cochemé, J.-J. (1996) Alteration of silicic vitric tuffs interbedded in volcaniclastic deposits of the Southern Basin and Range Province, Mexico; evidences for hydrothermal reactions. *Clays and Clay Minerals*, **44**, 49–67.

Patino, L.C., Velbel, M.P.R., Price, J.R., and Wade, J.A. (2003) Trace element mobility during spheroidal weathering of basalts and andesites in Hawaii and Guatemala. *Chemical Geology*, **202**, 343–364.

Pearce, J.A. and Cann, J.R. (1973) Tectonic setting of basic volcanic rocks determined using trace element analyses. *Earth and Planetary Science Letters*, **19**, 290–300.

Rollinson, H. (1993) *Using Geochemical Data; Evaluation, Presentation, Interpretation*. Longman Scientific and Technical, Harlow, Essex, UK, 352 pp.

Ronov, A.B., Balashov, Y.A., and Migdisov, A.A. (1967) Geochemistry of the rare-earths in the sedimentary cycle. *Geochemistry International*, **4**, 1–17.

Rubin, J.N., Henry, C.D., and Price, J.G. (1993) The mobility of zirconium and other 'immobile' elements during hydrothermal alteration. *Chemical Geology*, **110**, 29–47

Salvi, S. and Williams-Jones, A.E. (1996) The role of hydrothermal processes in concentrating high-field strength elements in the Strange Lake peralkaline complex, northeastern Canada. *Geochimica et Cosmochimica Acta*, **60**, 1917–1932.

Salvi, S., Fontan, F., Monchoux, P., Williams-Jones, A.E., and Moine, B. (2000) Hydrothermal mobilization of high field strength elements in alkaline igneous systems: evidence from the Tamazeght Complex (Morocco). *Economic Geology*, **95**, 559–576.

Saunders, A.D., Tarney, J., Marsh, N.G., and Wood, D.A. (1980) Ophiolites as ocean crust: a geochemical approach. Pp. 193–204 in: *Ophiolites: Proceedings of the International Ophiolite Symposium* (A. Panayiotou, editor). Ministry of Agriculture and Natural Resources, Cyprus, 1979. Geological Survey Department, Cyprus.

Schilling, J.G. (1973) Iceland Mantle Plume: geochemical study of Reykjanes ridge. *Nature*, **242**, 565–571.

Senkai, A.L., Dixon, J.B., Hossner, L.R., Abder-Ruhman, M., and Fanning, D.S. (1984) Mineralogy and genetic relationships of tonstein, bentonite, and lignite strata in the Eocene Yegua Formation of east-central Texas. *Clays and Clay Minerals*, **32**, 259–271.

Shirozu, H. and Iwasaki, T. (1980) Clay minerals in alteration zones of Kuroko deposits, with special reference to montmorillonite. *Journal of the Japanese Association of Mineralogists, Petrologists and Economic Geologists, Special Issue* **2**, 115–121 (in Japanese).

Sun, S.S. and McDonough, W.F. (1989) Chemical and isotopic systematics of oceanic basalts: implications for mantle composition processes. Pp. 313–345 in: *Magmatism in the Ocean Basins* (A.D. Saunders and M.J. Norry, editors). Special Publication **42**, Geological Society, London.

Sverjensky, D.A. (1984) Europium redox equilibrium in aqueous solution. *Earth and Planetary Science Letters*, **67**, 70–78.

Terkado, Y. and Fujitani, T. (1998) Behavior of rare earth elements and other trace elements during interactions between acidic hydrothermal solutions and silicic volcanic rocks, southwestern Japan. *Geochimica et Cosmochimica Acta*, **62**, 1903–1917.

Torres-Alvarado, I.S., Pandarinath, K., Verma, S.P., and Dulski, P. (2007) Mineralogical and geochemical effects due to hydrothermal alteration in the Los Azures geothermal field, Mexico. *Revista Mexicana De Ciencias Geologicas*, **24**, 15–24.

Velde, B. (1985) *Clay Minerals: A Physico-Chemical Explanation of their Occurrence*. Developments in Sedimentology, **40**, Elsevier, Amsterdam, 427 pp.

Weaver, C.E. (1989) *Clays, Muds, and Shales*. Developments in Sedimentology, **44**, Elsevier, Amsterdam, 819 pp.

Weaver, C.E. and Pollard, L.D. (1973) *The Chemistry of Clay Minerals*. Developments in Sedimentology, Elsevier Science Publishing, Amsterdam, 213 pp.

Whitney, D.L. and Evans, B.W. (2010) Abbreviations for names of rock-forming minerals. *American Mineralogist*, **95**, 185–187.

Wilson, M.J. (1987) X-ray powder diffraction methods. Pp. 26–98 in: *A Handbook of Determinative Methods in Clay Mineralogy* (M.J. Wilson, editor). Blackie and Sons Ltd, Glasgow, UK.

Winchester, J.A. and Floyd, P.A. (1977) Geochemical discrimination of different magma series and their differentiation products using immobile elements. *Chemical Geology*, **20**, 245–252.

Wise, S.W. and Kelts, K.R. (1972) Inferred diagenetic history of a weakly silicified deep sea chalk. *Transactions of the Gulf Coast Association of Geological Societies*, **22**, 177–203.

Yalçın, H. and Gümüşer, G. (2000) Mineralogical and geochemical characteristics of Late Cretaceous bentonite deposits of the Kelkit Valley Region, Northern Turkey. *Clay Minerals*, **35**, 807–825.

Yıldız, A. and Dumlupınar, İ. (2009) Mineralogy and geochemical affinities of bentonites from Kapıkaya (Eskişehir, western Turkey). *Clay Minerals*, **44**, 339–360.

Yılmaz, Y., Tüysüz, O., Yiğitbaş, E., Genç, Ş.C., and Şengör, A.M.C. (1997) Geology and tectonic evolution of the Pontides. Pp. 183–226 in: *Regional and Petroleum Geology of the Black Sea and Surrounding Region* (A. Robinson, editor). AAPG Memoir, **68**, American Association of Petroleum Geologists, Tulsa, Oklahoma.

Zielinski, R.A. (1982) The mobility of uranium and other elements during alteration of rhyolite ash to montmorillonite: a case study in the Troublesome Formation, Colorado, U.S.A. *Chemical Geology*, **35**, 185–204.

(*Received 16 November 2009; revised 16 March 2011; Ms. H. Dong; A.E. 377*)